

1 **Dissolved greenhouse gases (nitrous oxide and methane) associated with the naturally iron-**
2 **fertilized Kerguelen region (KEOPS 2 cruise) in the Southern Ocean**

3
4 **L. Farías^{1*}, L. Florez-Leiva², V. Besoain^{1,3}, G. Sarthou⁴, and C. Fernández⁵**

5
6 ¹Departamento de Oceanografía. Universidad of Concepción and Centro de Ciencia del Clima y la
7 Resiliencia (CR)², Chile

8
9 ²Programa de Biología. Universidad del Magdalena, Santa Marta, Colombia

10
11 ³Escuela de Ciencias del Mar, Pontificia Universidad Católica de Valparaíso, Chile

12
13 ⁴LEMAR-UMR 6539, CNRS-UBO-IRD-IFREMER, Place Nicolas Copernic, 29280 Plouzané, France

14
15 ⁵Sorbonne Universités, UPMC Univ Paris 06, UMR 7621, Laboratoire d'Océanographie Microbienne,
16 Observatoire Océanologique, F-66650 Banyuls/mer, France and Department of Oceanography, COPAS
17 SA program and Interdisciplinary Center for Aquaculture Research (INCAR), University of
18 Concepción, Chile

19
20
21 Correspondence should be addressed to:

22 Laura Farias; lfarias @profc.udec.cl

23

24

25

26

1 **ABSTRACT**

2 The concentrations of greenhouse gases (GHGs), such as nitrous oxide (N₂O) and methane (CH₄), were
3 measured in the Kerguelen Plateau Region (KPR). The KPR is affected by an annual microalgal bloom
4 caused by natural iron fertilization, and this may stimulate the microbes involved in GHG cycling. This
5 study was carried out during the KEOPS 2 cruise during the austral spring of 2011. Oceanographic
6 variables, including N₂O and CH₄, were sampled (from surface to 500 m depth) in two transects along
7 and across the KRP, the north-south (TNS) transect (46°-51°S, ~72°E) and the east-west (TEW)
8 transect (66°-75°E, ~48.3°S); both associated with the presence of a plateau, Polar Front (PF) and other
9 mesoscale features. The TEW presented N₂O levels ranging from equilibrium (105%) to slightly
10 supersaturated (120%) with respect to the atmosphere whereas CH₄ levels fluctuated dramatically, being
11 highly supersaturated (120-970%) in areas close to the coastal waters of Kerguelen Island and in the PF.
12 The TNS showed a more homogenous distribution for both gases, with N₂O and CH₄ levels ranging
13 from 88% to 171%, and 45% to 666% saturation, respectively. Surface CH₄ peaked at southeastern
14 stations of the KPR (A3 stations) where a phytoplankton bloom was observed. Both gases responded
15 significantly, but in contrasting ways (CH₄ accumulation and N₂O depletion), to the patchy distribution
16 of chlorophyll a. This seems to be associated to the supply of iron from various sources. Air-sea fluxes
17 for N₂O (from -10.5 to 8.65, mean 1.25±4.04 μmol m⁻² d⁻¹) and for CH₄ (from 0.32 to 38.1, mean
18 10.01±9.97 μmol⁻² d⁻¹) indicated that the KPR is both a sink and a source for N₂O, and a considerable
19 and variable source for CH₄. This appears to be associated with biological factors, as well as the
20 transport of water masses enriched with Fe and CH₄ from the coastal area of the Kerguelen Islands.
21 These previously unreported results for the Southern Ocean suggest an intense microbial CH₄ production
22 in the study area.

23 **Keywords:** Nitrous oxide, methane, dissolved iron fertilized Kerguelen area, mesoscale structures and
24 polar front Southern Ocean.

1 1. Introduction

2 The increasing concentration of greenhouse gases (GHGs) in the troposphere, such as CO₂, N₂O and
3 CH₄, affect the Earth's radiative balance. Additionally, the increasing concentration of ozone-depleting
4 gases (such as chlorofluorocarbons and N₂O) in the stratosphere is weakening the ozone shield,
5 permitting higher levels of damaging ultraviolet radiation to reach the Earth's surface. The relative
6 potency of a GHG is determined by its respective residence time in the atmosphere (Cicerone and
7 Orelamland, 1988), and the extent of magnitude of emissions to the atmosphere, of which the
8 input/contribution from the ocean is considered to be important (IPCC, 2013).

9 Although oceans are generally considered to be a net source of GHGs to the atmosphere, for example of
10 N₂O and CH₄, the oceanic distribution of these GHGs and the amount exchanged via the air-sea
11 interface is highly variable (Nevison et al., 1995; Holmes et al., 2000; Rhee et al., 2009). Thus, source
12 and sink behaviors of GHGs have been observed on different spatial and temporal scales. In general
13 terms, these behaviors depend on biological and physical processes that promote outgassing or
14 sequestering mechanisms. Physical and biological features of the Southern Ocean suggest the existence
15 of a potential for both the production and removal of CH₄ and N₂O (Rees et al., 1999; Tilbrook and Karl,
16 1994), although very little information on dissolved N₂O and CH₄ distributions is currently available for
17 the region. The substantial spatial variation in regional gas exchange could be due to the increased gas
18 solubility in low-temperature Subantarctic waters, combined with either the downwelling associated
19 with intermediate and deep water formation in the Northern and Southern part, respectively, of the
20 Antarctic Zone. Additional further variation may be caused by the upwelling of deep and intermediate
21 waters in the southern part of the Polar Frontal Zone (Park and Vivier, 2012).

22 In different regions of the Southern Ocean, the surface layer is permanently supersaturated with CH₄
23 (Bates et al. 1996; Tilbrook and Karl, 1994, Toshida et al., 2011), but this is not the case for N₂O, which

1 may occur in either under- or super saturated conditions Law and Ling, 2001, Rees et al., 1997, Zhan
2 and Chen, 2009). Aside from physical processes affecting GHG concentrations in the water column and
3 their concomitant air-sea fluxes, the concentrations also depend on organic matter (OM) availability and
4 oxygen levels, which determines whether aerobic or anaerobic respiration occurs (Codispoti et al., 2001;
5 Reeburgh, 2007). The availability of dissolved iron (dFe) should also be included as a direct variable
6 affecting the recycling of GHG's (through production and consumption), as several Fe-containing
7 enzymes are required for GHG cycling, which are involved in the electron transfer chains in bacterial
8 respiratory systems and Nitrogen cycling (Arrieta et al., 2004; Kirchman et al., 2003; Morel et al.,
9 2003a). Indirectly, dFe stimulates ocean productivity which can enhance carbon and nitrogen export
10 from the euphotic zone to the subsurface (Boyd and Ellwood, 2010), resulting in an increase in
11 microbial activities and mediate GHG production via nitrification (Fuhrman and Capone, 1991).
12 N₂O is mainly produced during the first step of nitrification (the aerobic oxidation of NH₄⁺ to NO₂⁻), and
13 during partial denitrification (the anaerobic reduction of NO₃⁻/NO₂⁻ to N₂O). N₂O can also be consumed
14 by complete denitrification via dissimilatory reduction to N₂ (Codispoti and Cristiensen, 1985), or
15 assimilatory N₂O reduction to NH₄⁺ (Farias et al., 2013). CH₄, on the other hand, is mainly formed by
16 methanogens during anaerobic OM degradation (Wuebbles & Hayboe, 2001) or by methylotrophs during
17 CH₄ formation derived from transformations of methyl-compounds such as methylphosphonate (MPn)
18 (Karl et al., 2008), dimethyl-sulphoniopropionate (DMSP) (Damm et al., 2010), and dimethylsulphide
19 (DMS) (Florez-Leiva et al., 2013). In addition, CH₄ can be consumed (oxidized) via aerobic
20 methanotrophy (Hanson and Hanson, 1996). Since Southern Ocean waters are well oxygenated, it is
21 thought that the dominant mechanisms of production in surface waters are by either through N₂O
22 formation by nitrification (Nevison et al., 2003) and CH₄ formation via either methanogenesis in
23 suspended particles (Scranton and Brewer, 1977) or methylotrophy (Sun et al., 2011).

1 The main objective of the present study is to describe for first time the N₂O and CH₄ contents in the
2 Southern Ocean under the influence of natural fertilization during the spring phytoplankton bloom in the
3 Kerguelen Plateau Region (KPR). The determination of the role of the Southern Ocean in CH₄ and N₂O
4 air–sea exchange may be critical in understanding the factors that influence GHG cycling. This includes
5 dFe which comes from different sources within the KPR, inducing mesotrophic conditions associated
6 with the coastal waters of Kerguelen Island and of the central Kerguelen plateau, an area of within the
7 Central Plateau area of the KPR that demonstrates an annually recurrent phytoplanktonic bloom in the (Blain et al., 2008; Chever et al., 2010), and with the Antarctic Polar front and other mesoscale structures
8 (Mongin et al., 2008, Lasbleiz et al., 2014).

10 2. Methods

11 2.1. Study area

12 Samples were collected within the Kerguelen Plateau Region or KPR (Fig. 1) during the KEOPS 2
13 cruise at stations along TNS (46°–51°S) and (TEW (66°–75°E). The cruise took place from October 11th
14 to December 11th, 2011, on board the research vessel (RV) *Marion-Dufresne*. Some of the stations were
15 located in the naturally Fe-enriched PFZ, in the coastal shelf waters of Kerguelen Island and within the
16 southeastern KPR bloom (including station A3 from the previous KEOPS 1 cruise). St. R-2 located east
17 of the Kerguelen plateau was considered to be typical of HNLC conditions (see Table 1). The positions
18 of the stations were selected according to a strategy based on real-time ocean color and altimetry
19 satellite images (d’Ovidio et al., 2015).

20 **2.2. Sampling:** Continuous vertical profiles of temperature, salinity, dissolved O₂, fluorescence and
21 Photosynthetically Active Radiation (PAR) were obtained using a conductivity temperature and depth
22 (CTD) sensor. Seawater samples were collected using a SeaBird SBE 911plus CTD unit mounted on a
23 24 12 L bottles rosette. Water samples for gases (N₂O, CH₄), nutrients, and pigments (sampled in this

1 consecutive order) were obtained from nine depths distributed between the surface and 500 m depth.
2 Water samples for CH₄ (triplicate) and N₂O (triplicate) analyses were taken in 20 mL glass vials and
3 poisoned with HgCl₂ (0.1 ml of saturated HgCl₂ solution per vial). Subsequently, the vials were sealed
4 with a butyl-rubber septum and an aluminum cap, avoiding bubble formation, and stored in darkness at
5 room temperature until laboratory analysis. Syringes of 50 mL were directly connected to the spigot of
6 the Niskin bottles to take nutrient samples (NO₃⁻, NO₂⁻, PO₄³⁻ and H₄SiO₄) at each sampled depth.
7 Duplicate samples were collected and drawn through a 0.45 μm Uptidisc adapted to the syringe, and
8 then immediately analyzed using an autoanalyzer (more details in Blain et al., 2014). Total chlorophyll-
9 a (*TChl-a*) samples in triplicate were filtered into a 25 mm glass- fiber filter (GF/F), and then
10 immediately frozen (-20°C). Samples were kept until later analysis by high performance liquid
11 chromatography (HPLC) (more details in Lasbleiz et al., 2014).

12 **2.3. Chemical analysis:** N₂O and CH₄ were analyzed by via the generation of a 5 mL ultra-pure Helium
13 headspace into the vial using a gastight syringe, then within the vial the gas and liquid phases were
14 equilibrated at 40°C, following this the gases within the vial were quantified through the use of a gas
15 chromatograph determined by Helium equilibration (5-mL Helium headspace and 15-mL of seawater) at
16 40°C, finally quantification via chromatography was carried out. N₂O was analyzed in a Varian 3380
17 Gas Chromatograph using an electron capture detector at 350°C and connected to an autosampler
18 device. CH₄ was analyzed in a Shimadzu 17A gas chromatograph using a flame ionization detector at
19 250°C through a capillary column GS-Q at an oven temperature of 30° C. A calibration curve was made
20 with four concentrations for N₂O (0.1 ppm, 0.32, 0.5 ppm, and 1 ppm, by Matheson standards) and four
21 concentrations for CH₄ (0.5, 1.78, 2 and 10 ppm, by Matheson standards). Both detectors linearly
22 responded to these concentration ranges. The analytical error for the N₂O and CH₄ analyses was less
23 than 3% and 5% respectively. The ECD and FID detectors lineally responded to these concentration

1 ranges and the analytical error for the N₂O measurements for this study was about 3%. The uncertainty
2 of the measurements was calculated from the standard deviation of the triplicate measurements by depth.
3 Samples with a variation coefficient higher than 10 % were not taken into account for the gas database.
4 More details regarding the analysis of both gases can be found in Farias et al. (2009). Nutrients were
5 immediately analyzed onboard by standard automated colorimetric methods (Tréguer and LeCorre,
6 1975) using the continuous flow autoanalyser (Skalar). The precision and detection limit of the method
7 was, respectively, ±50 nM and 20 nM for NO₃⁻, and ±30 nM and 110 nM for PO₄⁻³⁻ (more details in
8 Blain et al., 2015). NH₄⁺ was measured by fluorometric analysis (Holmes et al., 2000) with a precision
9 of ±50 nM.

10 **2.4. Data analysis:** To interpret the vertical variation of N₂O and CH₄, and assess how biogeochemical
11 processes may affect their concentrations, the water column was divided into two layers according to
12 density gradient: (1) well-mixed and (2) subsurface from the base of the mixed layer (ML) to 500 m
13 (arbitrary depth used only for comparison proposes). Nutrient inventories for TChl-*a*, N₂O and CH₄
14 were calculated by numerical integration of data with linear interpolation at intervals of one meter, based
15 on at least 4-6 sampled depths per layer. Saturation percentages of gases were calculated from the
16 measured CH₄ and N₂O concentrations and those estimated to be in equilibrium with the current gas
17 concentrations in the atmosphere register (NOAA/ESRL program
18 <http://www.esrl.noaa.gov/gmd/hats/combined/N2O.html>) based on *in situ* temperature and salinity
19 records according to the solubility parameterization of CH₄ (Wiesenburg and Guinasso, 1979) and N₂O
20 (Weiss and Price, 1980). GHG flux through the air-sea interface was determined using the following
21 equation, modified by Wanninkhof (1992):

$$F = kw(T^\circ, salinity) \cdot (C_w - C_a)$$

1 where k_w is the transfer velocity from the ML to the atmosphere, as a function of wind speed,
2 temperature and salinity in the ML according to parametrization; C_w is the mean gas concentration in the
3 mixed layer; while C_a is the gas concentration in the mixed layer expected to be in equilibrium with the
4 atmosphere. Since gas transfer velocity is related to wind speed, this was calculated according to the
5 well-known exchange models of Liss and Merlivat (1986) or LM86 and Wanninkhof (1992) or W92,
6 based on the dependence of the transfer velocity on wind speed. Wind speed and direction were obtained
7 from the ship's meteorological station. Wind speed was estimated as a moving seven day average prior
8 to the sampling period in order to smooth out short-term fluctuations and highlight longer-term trends.
9 The mixed layer depth was calculated using a potential density-based criterion, defining the mixed layer
10 depth (ML) as the shallowest depth at which density increased by 0.02 kg m^{-3} from the sea surface
11 value.

12 Pearson product-moment correlations (r_s) were determined for GHG, and *TChl-a* and nutrient
13 inventories were estimated for both the ML and for the whole water column from the surface to 500 m
14 depth. The threshold value for statistical significance was set as $p < 0.05$. A principal component analysis
15 (PCA) using the empirical orthogonal function (EOF; Emery and Thomson, 1997) was performed to find
16 the co-variability patterns of a number of stations located in spatial gradients in terms of nutrients, gases
17 (O_2 , N_2O , and CH_4), *TChl-a*, and dFe. This analysis excluded the stations from the NS transect as no
18 measurements were recorded (Qu  rou   et al, 2015). PCA were made with all biogeochemical variables
19 measured in the ML and with these variables obtained in the water column from the surface to a depth of
20 500 m, in order to detect differences in the vertical structure.

21

22

23

1 **Results**

2 **3.1. Oceanographic conditions.**

3 Oceanographic characteristics of the sample stations during the KEOPS 2 cruise are shown in Table 1.

4 Two transects, carried out almost synoptically across and along the KPR (survey region – Fig. 1) were
5 undertaken to establish the position of the main mesoscale structures as fronts (Fig. 2). The Polar Front
6 (PF) crosses the KPR and denotes certain physical structures (i.e. convergence processes) visible
7 throughout temperature and salinity (Park and Vivier, 2012).

8 Regarding the TEW (66° to 75°E, along 47°S), vertical cross sections of temperature and salinity along
9 with a T-S diagram are illustrated in Fig 2 (a, c, e). Temperature and salinity varied between 2.41° and
10 3.30°C, and between 33.60 and 34.67, respectively. A weak structure with colder and fresher surface
11 waters was registered in the PF, which crossed these transects twice, at ~71°E (St. TEW-3,-4) and at
12 ~73.5°E (St. TEW-7, -8). Middle stations (Sts. TEW-4, -5 and E) are located in an area with a complex
13 recirculatory system. This is a superficial section inundated by mixed Antarctic surface water (AASW)
14 and coinciding with an area of a PF northward inflexion (Fig. 1). The presence of Subantarctic mode
15 water (SAMW) was observed east of 73.5° E (Sts. TEW-7, -8, Fig. 2f). In addition, a marked variability
16 in subsurface water was observed, attributed to the mixing of water masses; this was particularly strong
17 in TEW within the PF, revealing a vertical mixing process produced by convergence, particularly
18 evident at St. TEW-7 (Fig. 2e). Regarding the TNS (46°-51°S, along ~72°E), Fig. 2 (b, d, f) shows
19 vertical cross sections of temperature, salinity and a T-S diagram, respectively. Temperature and salinity
20 fluctuated from 1.67° to 4.17°C and from 33.67 to 34.68, respectively, and a gradual decrease in
21 temperature and an increase in salinity were observed in the surface layer from north to south (Fig 2 b,
22 d). A water parcel of a relatively cold water mass was observed to be spreading northward in subsurface
23 waters. This is noted as an expression of the PF, which marks the location where the AASW moves

1 northward, descends rapidly, and sinks below 200 m depth (Fig. 2 b). These distributions coincided with
2 the expected water mass distribution, this being the case for the northern (Sts. TNS-1,-2) and southern
3 (Sts. A3, TNS-10) stations, mainly occupied from the surface to 250 m by the SAMW and the AASW,
4 respectively (Fig 2f).

5 **3.2. Biogeochemical variables**

6 Figure 3 shows vertical cross sections along the TEW of biogeochemical variables including nutrients
7 (only NO_3^- and PO_4^{3-}), *TChl-a*, O_2 and GHGs. The surface layer continuously showed NO_3^-
8 concentrations, fluctuating from 22 to 27 $\mu\text{mol L}^{-1}$ (typical condition of the AASW). However, a relative
9 depletion of NO_3^- was observed at the stations located north and eastward of the PF (Fig 3a). PO_4^{3-}
10 presented the same pattern as NO_3^- and the N:P ratio of dissolved nutrients averaged around 14.5, with
11 the exception of some values of 13.2 from stations located close to the PF (Fig. 3 b). *TChl-a* fluctuated
12 from 0.005 to 4.69 $\mu\text{g L}^{-1}$ and peaked at Sts. TEW-1, -2 (both located in a coastal area 10 and 75 km
13 away from Hillsborough Bay coast) and Sts. TEW-7,-8 (to the north of PF). *TChl-a* showed a relative
14 decrease at stations located in the Central Section (Fig. 3c). O_2 concentration varied from 320 μM (in
15 surface water) to 185 μM (at 500 m depth), consistently maintaining super saturation conditions (Fig
16 3d).

17 N_2O fluctuated from 14.0 to 25.4 nmol L^{-1} (equivalent to a range of 102-182.2% saturation, Fig 3e).
18 Superficially, in the western and central section (70.5- 73°E) the N_2O concentration was close to
19 equilibrium with the atmosphere in surface waters, and in surface waters at sites where the PF crosses
20 the transect, i.e. Sts. TEW-4 and TEW-7 (Fig. 3e) N_2O was slightly undersaturated (around 90%). N_2O
21 levels increased slightly attaining around 120% saturation towards the subsurface water. CH_4 ranged
22 from 1.4 to 31.35 nmol L^{-1} , equivalent to a saturation range of 43-969%. In contrast to N_2O , surface
23 waters were always supersaturated in CH_4 , demonstrating the greatest increase in gas levels (up to

1 970%) in coastal waters close to Kerguelen Island, a relative decrease (<200% saturation) in the central
2 section (between 71° and 73. Seasonal and inter-annual variability of biogeochemical variables,
3 including nitrous oxide (N₂O) an important climate active gas, were analyzed during monthly
4 observations between 2002 and 2012 at the COPAS Ocean Time-Series station in the coastal upwelling
5 area off central Chile (36° 30.8' S). Oxygen, N₂O, nutrients and chlorophyll-a (*TChl-a*) showed clear
6 seasonal variability associated with upwelling favorable winds (spring-summer), and also inter-annual
7 variability, which in the case of N₂O was clearly observed during N₂O hotspot occurrence with
8 saturation levels of up to 4849%. The hotspots consistently occurred during the upwelling-favorable
9 period in years 2004, 2006, 2008, 2010 and 2011, below to the mixed layer (15-50 m depth) in waters
10 with hypoxia and specific NO₂⁻ accumulation. They displayed a 3 times greater apparent N₂O production
11 (ΔN₂O) than the average monthly anomalies (2002-2012). Estimated relationships of ΔN₂O vs. apparent
12 oxygen utilization (AOU) and ΔN₂O vs. NO₃⁻ suggest that aerobic ammonium oxidation (AAO) and
13 partial denitrification are the processes responsible for high N₂O accumulation in subsurface water.
14 *TChl-a* levels correlated fairly well with the presence of the N₂O hotspots, suggesting that microbial
15 activities, facilitated by a higher availability of organic substrates, trigger high N₂O levels. This in turn
16 results in a huge efflux into the atmosphere of up to 260 μmol m⁻² d⁻¹. N₂O hotspots are transient events
17 or hot moments, which may occur more frequently than they are observed. If so, this upwelling area is
18 producing and emitting greater than expected amounts of N₂O and resulting in an important source of
19 N₂O that should be considered in the global atmospheric N₂O balance. 5°S, or Sts. TEW-4, -5 and E2),
20 and a strong increase (up to 778%) at St. TEW-7. Remarkably, CH₄ concentrations in subsurface waters
21 were low compared to the surface waters (Fig. 3f).

22 Vertical cross sections of biogeochemical variables along the TNS are shown in Figure 4. NO₃⁻ and
23 PO₄³⁻ gradually increased from north to south from 24 to 30 μmol L⁻¹ and from 1.5 to 2 μmol L⁻¹,

1 respectively (Fig 4 a, b). This spatial trend coincided with the expected transition of water mass
2 dominance and its mixing between the SAMW and the AASW (Fig 2 f). *TChl-a* ranged from 0.005 to
3 2.391 $\mu\text{g L}^{-1}$ and peaked in the southernmost stations (Sts. TNS-8, -9 and A3-2; Fig. 4b) and coincided
4 with a slight increase in nutrients. There a deep Fe-enriched and lithogenic silica reservoir seemed to
5 influence the area (Lasbleiz et al., 2014; Qu  rou   et al., 2015). O_2 distribution was similar to that
6 observed in the WE transect.

7 N_2O concentrations ranged from 12.37 to 23.8 nmol L^{-1} , equivalent to 88.5% to 171% saturation. N_2O
8 levels close to equilibrium or undersaturation were often observed in surface waters, except at St.
9 TNS08 (Fig. 4e). CH_4 varied from 1.47 to 21.88 nM, or 45 to 666% saturation, and peaked in southern
10 stations (Fig 4f). Notably, high levels of *TChl-a* were associated with high concentrations of CH_4 in this
11 transect. Southern stations had extremely low N_2O concentrations (less than 6.9 nM or 70% saturation),
12 such as St. A3, which is located in an area of relatively high dFe availability and within a phytoplankton
13 bloom.

14 PCA, including dFe and GHG data were obtained from the TEW as shown in Figure 5. The results did
15 not change when O_2 was removed from the analysis, indicating that O_2 availability does not modify the
16 percentage of the variance. When the data set used in the PCA is restricted to the ML (Fig. 5a), stations
17 located on the TEW were grouped into three sets, clearly separating stations located in eastern (north of
18 the PF, St. TEW-7), western, and coastal areas (TEW-1,-2), and within the central section (Sts. TEW-4,
19 -5, E2). The variability among stations can be predominantly explained by the first component,
20 accounting for 75.7% of the variance. Figure 5 suggests possible interpretations of the relationships
21 between the variables with their respective weights assigned to each of them (illustrated with an
22 eigenvector). The figure shows a close relationship between N_2O , nutrients, CH_4 , dFe and *TChl-a*. The

1 PCA analysis using data from the entire water column and provided a similar grouping of the sample
2 stations (Fig 5b).

3 **3.3. Vertical distribution of gases and other variables at selected stations**

4 Figure 6 shows typical profiles of oceanographic and biogeochemical variables (including gases).
5 Stations were separated *a priori* according to biogeochemical (PCA analysis for the case of the TEW;
6 Fig.5) and oceanographic criteria (T-S diagram, Fig. 2e, f). Selected stations included: Sts. A3, with a
7 recurrent annual bloom (historical station sampled in KEOPS 1, Blain et al., 2007) and moderate dFe
8 levels ($\sim 0.18 \text{ nmol L}^{-1}$). Some stations displayed evidence of an active uptake of dFe; St. TEW-7 had
9 one of the highest dFe ($\sim 0.40 \text{ nmol L}^{-1}$) and TChl-*a* levels, and also showed evidence of rapid dFe
10 uptake (Fourquez et. 2014). For comparative purpose, we include the most northern station of the TNS
11 (St. TNS01), St. R-2 (in the HNLC area), and a coastal station close to Kerguelen Island, which had the
12 highest dFe levels (up to 3.82 nmol L^{-1}). Vertical distribution of N₂O and CH₄ clearly varied, while
13 elevated CH₄ concentrations were generally observed superficially and in the ML base, and
14 concentrations decreased with increased depth, whereas N₂O concentrations gradually increased with
15 depth. Gas contents also differed between stations and were observed to correlate in a similar way with
16 with TChl-*a* and dFe levels.

17 The stations located at the extremities of the TEW (i.e., TEW-1 and TEW-7) had the highest CH₄ levels
18 (Fig 6), while N₂O levels were relatively low. Conversely, Sts. TNS-1 and A3-2 located in the extreme
19 north and south of the TNS presented relatively low levels of CH₄ compared to the TEW. Station R-2,
20 which is located in the HNLC area had the lowest N₂O and CH₄ content, and both gases were
21 homogeneously distributed with depth (Fig. 6). This is consistent with TChl-*a* levels of less than $0.5 \mu\text{g}$
22 L^{-1} .

23 **3.4. Nutrient, TChl-*a*, dFe and GHG inventories and air-sea GHG exchanges**

1 Table 2 shows the inventories of NO_3^- , PO_4^{3-} and GHGs in the ML and the water column from the
2 surface to 500 m; mean GHG concentrations in the ML, wind speed, and air-sea GHG fluxes are also
3 included. ML depths varied widely from 16 m (at the station near Kerguelen Island) to 181 m. The
4 *TChl-a* pool, estimated on the basis of the photic layer, fluctuated from 8.77 to 75.45 mg m^{-2} . Levels
5 were notably elevated at Sts. SPF and A3-2 (up to fivefold greater), in comparison to the more
6 oligotrophic stations such as St. R-2. Surface NO_3^- and PO_4^{3-} inventories did not show significant
7 differences among stations and varied between 1.56 to 16.03 and 0.13 to 1.07 mol m^{-2} , respectively.
8 Minimal values were registered at stations St. TEW-7--8 and TNS-1, both located north of the PF.
9 N_2O pools varied from 0.201 to 2.55 and from 1.12 to 10.05 mmol m^{-2} in the ML and the whole water
10 column, respectively. Minimum values were registered in the ML at stations within the PF and also to
11 the north. These surface pools did not significantly correlate with *TChl-a*, but correlated strongly and
12 negatively with nutrients (r_s : 0.91 $p < 0.001$ for NO_3^- and r_s : 0.92, $p < 0.001$ for PO_4^{3-}). CH_4 inventories
13 fluctuated between 0.19 and 3.31 mmol m^{-2} for the ML, and 1.06 and 7.44 mmol m^{-2} for the whole water
14 columns. Once again, inventories in the ML were two and fivefold higher at Sts. TEW-7 and A3-2,
15 respectively, than at St. R-2. CH_4 inventories were four and sevenfold higher in Sts. TEW-7 and A3-2,
16 respectively, than at St. R-2. The comparison between the CH_4 inventories (standardized by the
17 thickness of the layer) obtained from the ML and from the entire water column indicates that the
18 maximum values came from the ML's base, remarkably in the PF (Table 2). CH_4 pools correlated
19 positively with *TChl-a* pools ($r_s = 0.69$; $p < 0.05$), but did not show any correlation with NO_3^- and PO_4^{3-} .
20 Thus, minimum values for both nutrients were found when *TChl-a* was higher.

21 Average hourly wind velocity during the cruise was $10.53 \pm 5.52 \text{ m s}^{-1}$, occasionally falling below 0.31
22 m s^{-1} or rising above 29.1 m s^{-1} . The ML depth did not show any significant relationship to wind speed
23 (r_s : 0.20 $p = 0.41$) or the water mass structure (Table 1 and Fig. 2), but seems to be related to the complex

1 mesoscale circulation observed in the KPR (Park et al., 2014; Zhou et al., 2014). N₂O fluxes, estimated
2 by LM86, fluctuated between -9.69 and 10.02 $\mu\text{mol m}^{-2} \text{d}^{-1}$ (mean: $1.25 \pm 4.04 \mu\text{mol m}^{-2} \text{d}^{-1}$), while those
3 estimated by W92 varied from -18.69 to 20.2 $\mu\text{mol m}^{-2} \text{d}^{-1}$ (mean: 2.41 ± 7.88). Substantial differences
4 were observed between the cubic (LM86) and the quadratic parameterizations (W92) during high wind
5 speeds; such as those measured during the N-S transect (21-23 October 2011, mean value of 12.08 m
6 s^{-1}), compared to those registered during the TEW (31 October – 02 November, mean value of 5.61 m
7 s^{-1}). The W92 increased in calculated fluxes by approximately a factor of two at high wind speeds, while
8 at low wind speeds the difference between LM86 and W92 was up to a factor of ~ 1.6 (see Table 2).
9 CH₄ fluxes varied from 0.21 to 38.1 $\mu\text{mol m}^{-2} \text{d}^{-1}$ (mean: 10.01 ± 9.97), and from 0.32 to 70.24 $\mu\text{mol m}^{-2}$
10 d^{-1} (mean: 21.27 ± 21.07), when LM86 and W92 were employed, respectively. At times the study area
11 acted as a source of very high CH₄ effluxes into the atmosphere, particularly at stations St. TNS-9 and
12 St. A3-2 where emissions were around three times as high as those calculated for St. R-2. There are
13 important differences between the two parameterizations, although the same trend was obtained among
14 stations (Table 2).

15 **4. Discussion**

16 Iron fertilization in the KPR influences phytoplankton growth and primary production (PP), and other
17 microbial activities (Cavagna et al., 2014; Christaki et al., 2014), as well as relative CH₄ accumulation
18 (Fig. 3f and Fig. 4f) and some N₂O depletion (Fig 3e). The gas distribution pattern clearly matched those
19 of Queroue et al. (2014) for *TChl-a* and PCA grouped stations using dFe. The segregation of stations
20 includes; the coastal area (Sts. TEW-1, -2), the PF (St. STEW-7) and the central plateau region (Sts. A3-
21 2). In the case of KEOPS 2, phytoplanktonic blooms were mainly represented by a microplanktonic
22 community (Lasbeiz et al., 2014), as those observed in the north Polar Front (St. TEW-7) and the central
23 part of the KPR (A3) stations displayed high rates of iron uptake (Qu  rou   et al., 2014). These

1 previously indicated areas, demonstrated variable but high particulate Fe of biogenic origin (van der
2 Merwe et al., 2014). This confirms an increased biological uptake which in turn determines a rapid dFe
3 turnover. The observed gas distribution patterns raise questions as to how the complex circulation and
4 some mesoscale structures support relatively high *TChl-a* accumulation and microbial activities in
5 comparison to surrounding waters, and particularly whether there are some fertilization mechanisms
6 (including the addition of Fe and nutrients) promotes GHG cycling and its associated microbial
7 activities.

8 **4.1. N₂O cycling**

9 Fuhrman and Capone (1991) pointed out the stimulation of ocean productivity through the addition of Fe
10 enhances nitrogen export from the euphotic zone to the subsurface layer and may result in enhanced
11 N₂O formation via the stimulation of nitrification. This stimulation may occur through the activation of
12 metallo-proteins that are involved in the various stages of ammonium and nitrite oxidation, as ammonia
13 oxidizing nitrifiers oxidize NH₄⁺ and NH₂OH to NO₂⁻ using iron-containing ammonia monooxygenase
14 (AMO) and hydroxylamine oxidoreductase (HAO), respectively (Morel et al., 2003b). Since N₂O is a
15 powerful greenhouse gas, 300 times more radiative than CO₂ per molecule, Fe addition could counteract
16 the climatic benefits of atmospheric CO₂ drawdown (Jain et al., 2000). The link between Fe fertilization
17 and enhanced N₂O formation via nitrification was supported by Law and Ling (2001), who found a
18 small but significant N₂O accumulation in the pycnocline during the Southern Ocean Iron Enrichment
19 Experiment (SOIREE) at 61°S, 140°E. Jin and Gruber (2003) subsequently predicted the long-term
20 effect of Fe fertilization on global oceanic N₂O emissions using a coupled physical-biogeochemical
21 model. Based on the model outputs, it was concluded that Fe fertilization induced N₂O emissions that
22 could offset the radiative benefits of the CO₂ drawdown. However, during other Southern Ocean Iron

1 Enrichment Experiments (EIFEX), Walter et al. (2005) found no N₂O enrichment after artificial Fe
2 fertilization.

3 Our findings revealed that natural Fe fertilization did not appear to stimulate N₂O accumulation in the
4 superficial layer (within the ML). There was no significant difference in the N₂O inventory estimates
5 from areas of higher accumulation of biomass with respect to those estimated for St. R-2, which was
6 used as a reference station (Table 2). Contrary to what was expected, no increase in N₂O content was
7 observed at stations close to Kerguelen Island (St TEW-1, TEW-2), which are highly enriched by dFe
8 from fresh water and sediments (Qu  rou   et al., 2014). This trend suggests that nitrifiers in surface water
9 are not being significantly stimulated by dFe supply from the sediments. In subsurface water (below
10 ML to 500 m depth) N₂O accumulation may be associated with nitrification and it is noted that dual
11 nitrate isotopic composition ($\delta^{15}\text{N-NO}_3^-$ and $\delta^{18}\text{O-NO}_3^-$) revealed an increase in both isotope values
12 with greater water depth in subsurface waters (100–400 m). This is a result of the partial consumption of
13 available nitrate in surface waters, the export of low $\delta^{15}\text{N}$ in Particulate Nitrogen (NP) and the
14 remineralization–nitrification that occurs in this situation (Dehairs et al., 2014). However, values of δ
15 $^{15}\text{N-NO}_3^-$ and $\delta^{18}\text{O-NO}_3^-$ in surface waters also suggests that nitrification is also occurring in surface
16 waters, but with a considerable variation.

17 Notably, the St. TEW-7, -8 and A3-2 were observed to be in equilibrium and slightly depleted in N₂O
18 (Fig. 3e; Table 2). It is likely that the explanation for this would be that the mixing process produced at
19 the PF (St. TEW-7) (with moderate levels of Fe, high levels of *TChl-a*, and evidence of active Fe
20 uptake) may stimulate the N fixers, as demonstrated by Mills et al. (2004), Berman-Frank et al. (2007),
21 and Moore et al. (2009). N-fixing microorganisms may have an effect on the N₂O inventory as they
22 could be used as an alternate substrate for fixers, as suggested by Farias et al. (2013). Thus, biological
23 N₂O fixation could be using and assimilating N₂O, producing N₂O depletion and a simultaneous

1 undersaturation. N-fixation has been observed in the cold waters of the Arctic and Antarctic (Blais et al.,
2 2012; Diez et al., 2012, Diez unpublished data), as well as in cold upwelled water (Fernandez et al.,
3 2011), suggesting that N₂O fixation may also occur more commonly than originally expected.
4 Coincidentally, St. TEW-7 (within the PF) also had the highest surface N-fixation (Gonzalez et al., 2014),
5 suggesting that N₂O is used as a substrate by diazotrophs (Farias et al., 2013) and that this process is
6 stimulated by enhanced Fe supply. N₂O undersaturation or equilibrium with the atmosphere was
7 observed in the TNS (Fig, 4e), particularly at stations north of the PF with influence from the SAMW.
8 This suggests that some kind of process occurring that removes or consumes gas from the upper water
9 column. A notable level of undersaturation was also observed at St. A3-2, which is located in the
10 recurring phytoplankton bloom and within a system of relatively high dFe concentration due to the
11 presence of the Plateau (Blain et al., 2007).

12 N₂O undersaturation has been reported, although rarely, in Polar and Sub-polar Ocean regions (Butler et
13 al., 1989; Law and Ling, 2001; Foster et al., 2009). Physical processes related with gas solubility and
14 deviations from the atmospheric equilibrium gas concentration could not explain the observed
15 undersaturation. It is probable that if the physical variables alter faster than that expected for gas
16 equilibrium with the atmosphere that there may be a gas deficit. Thus, deviation from the equilibrium
17 condition could be caused by rapid heating or cooling, refreshing, and/or a mixing of water masses
18 (Sarmiento and Gruber, 2006). An analysis of these potential changes was made for the AASW and the
19 SAMW. A cooling (decreasing T°C > 3) or fresh water influence (decreasing S from 34 to 10) would be
20 required to produce the observed undersaturation, neither of which was observed during the sampling
21 (Table 1), or expected during this season (Park et al., 2014). Additionally, if the two water masses were
22 mixed proportionally, as they are, the resulting process cannot produce undersaturation in regards to the
23 original N₂O levels and the signature temperature and salinity. Recently, Chen et al. (2014) reported that

1 surface water of the Indian sector of the Southern Ocean were understaturated in N_2O , suggesting a N_2O
2 influx. This phenomenon in the surface water may result from the intrusion of freshwater from ice melt
3 and the northeastward transport of the AASW. However, in the KPR, N_2O undersaturation seems to be
4 located in an area of high particle concentration under the influence of the SAMW (northern the PF),
5 Thus, a preliminary analysis indicates that biological processes are responsible for the N_2O
6 undersaturation and the concomitant influx from the atmosphere. In contrast, subsurface waters have
7 higher N_2O concentrations (saturations from 120% to 180%) than surface waters, which indicate a net
8 accumulation. In this case the most likely process responsible for N_2O accumulation is aerobic
9 ammonium oxidation (Codispoti et al., 2001), but no significant difference was noted at the stations with
10 the highest *TChl-a* levels, indicating that N_2O production by nitrification was not substantially
11 stimulated at those stations.

12 **4.2. CH_4 cycling**

13 There have been few studies on CH_4 distribution and production in the Southern Ocean (Lamontagne et
14 al., 1973; Tilbrook and Karl, 1994; Heeschen et al., 2004). Surface water in the Southern Ocean has
15 been reported to be undersaturated or lightly saturated with respect to atmospheric CH_4 , as a result from
16 the entrainment of CH_4 depleted deep water into surface water and from the seasonal ice covers acting as
17 a barrier for gas exchange (Toshida et al., 2011). Regarding the effect of iron addition on CH_4 cycling,
18 Wingenter et al. (2004) found low levels of CH_4 production (less than 1%) during artificial Southern
19 Ocean Fe enrichment experiments (SOFex). Simulated large-scale Southern Ocean Fe fertilization (OIF)
20 also resulted in anoxic conditions which may favor anaerobic methanogenesis (Oschlies et al., 2010).
21 However, our results show that surface and subsurface waters are supersaturated in CH_4 with a fourfold
22 enrichment in CH_4 with respect to the control area (Fig. 3e), this was associated to areas with elevated
23 *TChl-a* levels and iron uptake by microbial communities (Fourquez et al., 2014). Results showed a

1 marked spatial differences in CH₄ content measured in the TEW and TNS (t-student: 3.21 p<0.001)
2 (Fig. 3f and 4f), and that surface CH₄ accumulation generally coincided with areas of relatively higher
3 dFe levels, which in turn favors primary production (PP). Likewise, the CH₄ accumulation at
4 pycnoclines (Fig. 6) indicates that most CH₄ came from accumulated particles sinking from the surface
5 water, as commonly observed by Holmes et al. (2000) in different marine systems. The PCA analysis,
6 which included the measurement of dFe revealed a close relationship between CH₄ accumulation and Fe
7 availability and clearly grouped in areas with different biogeochemical characteristics. The fact that the
8 western and eastern sections showed high Fe levels (Quéroué et al., 2014,) relative to the Central Section
9 of the W-E transect, and that these sections had high CH₄ levels, which suggests that Fe stimulates CH₄
10 production. A similar situation occurs in Sts.A3 with high *TChl-a* levels and PP rates, as shown by
11 Cavagna et al. (2014). For example, station A3-2 and TEW-7 (maximum *TChl-a*) had the highest
12 integrated primary production rates (up to 3380 mg m⁻² d⁻¹) and the lowest C export level of around 2-
13 3% (Cavagna et al., 2014), this suggests an intense level of PP supported by regenerated N sources.
14 These contrast with the observed situation at St. R-2 with the lowest rate of regenerated production (with
15 a PP rate of around 135 mg m⁻³ d⁻¹ and an exported C rate of around 25% of PP).
16 Two hypotheses exist for CH₄ production in surface waters; One is that production only occurs in
17 association with anoxic particles (Karl and Tilbrook, 1994), produced for the most part by grazing
18 zooplankton, as methanogenic bacteria were considered to be present in an anaerobic microenvironment
19 in organic particles (pellets) or in the guts of zooplankton (Alldredge and Cohen, 1987; Karl and
20 Tilbrook, 1994). The other hypothesis was formulated more recently, that phytoplankton blooms should
21 favor zooplankton grazing process and/or stimulate bacterioplankton activity as CH₄ is generated via the
22 degradation of organic methyl compounds by bacteria (Karl et al., 2008).

1 Increased grazing of microbes by microzooplankton, as observed by Christaki et al. (2014), may
2 contribute to particle recycling (rich in organic carbon and DMSP), and increase the potential for
3 methanogenesis (Weller et al., 2013). Yoshida et al. (2011) found that high CH₄ production in the
4 Southern Ocean probably resulted from the grazing processes of Antarctic krill and/or from zooplankton
5 that feed on phytoplankton, and the subsequent microbial methanogenesis. This agrees with the findings
6 of sites enriched with iron and biomass that exhibit high carbon fluxes at 100 m depth, dominated by
7 large fecal pellets rather than phytodetrital aggregates (Laurenceau et al., 2014).

8 Conversely, aerobic CH₄ production in the water column could be associated with heterotrophic
9 activities. Christaki et al. (2014) showed that the highest bacterial production rates (up to 110 mg C m⁻²
10 d⁻¹), and the greatest abundance of heterotrophic bacteria were associated with stations where the
11 phytoplankton bloom was developed (TEW-7 and A3-2). Recent evidence indicates that methylotrophs
12 are candidates for mediated CH₄ generation using methylated compounds as DMSP and DMS (Florez-
13 Leiva et al., 2013; Weller et al., 2013). Among these heterotrophic microorganisms DMS degradation
14 can be ascribed to methylotrophic bacteria (Vissher et al., 1994) that derives energy from the conversion
15 of methyl into other products, as well as using S as a source for methionine biosynthesis (Kiene et al.,
16 1999). Current studies of natural and cultivated SAR11 alphaproteobacteria (strain Ca. *P. ubique*
17 HTCC1062; Sun et al., 2011) indicate that these microorganisms, among the most abundant
18 heterotrophic bacteria in surface waters, possess genes that are encoded for oxidation pathways of a
19 variety of one-carbon compounds, and have the capacity for demethylation and C1 oxidation, but do not
20 incorporate C1 compounds as biomass. This suggests that there is a close relationship between
21 phytoplankton, the only producers of DMSP (Yoch, 2002), and microbial communities which may be
22 recycling DMS. Phyto- and bacterioplankton relationships control DMS turnover, which could result in
23 several mechanisms of DMSP/DMS degradation (Simó et al., 2002; Vila-Costa et al., 2006) and produce

1 CH₄ (Damm et al., 2010; Florez-Leiva et al., 2013; Weller et al., 2013). These publications show that
2 phytoplankton species composition and biomass in different bloom phases, as well as eddy dynamics,
3 were important determinants of CH₄ saturation and emission.

4 With regards to the distribution, vertical profiles of the gas indicate that most CH₄ is being formed at the
5 surface and at pycnoclines (at the base of the ML), and consumed at subsurface and intermediary depths
6 (Figure 6). Thus, CH₄ distribution appears to be controlled largely by biological mechanisms rather than
7 by mixing, contrary to what has been reported by Heeschen et al. (2004). In general, surface waters of
8 the Southern Ocean were undersaturated with respect to atmospheric CH₄ as the result of the entrainment
9 of CH₄ depleted deep water to the surface and from seasonal ice cover acting as a barrier for gas
10 exchange. We observed CH₄ undersaturation, fluctuating between 40% and 90%, at most sampled
11 stations at depths of > 200. It is unlikely that this undersaturation results from the entrainment of CH₄
12 depleted waters that have high levels of gas solubility, but instead by a biological consumption as it is
13 more likely that a biological mechanism is involved. The only known process able to consume CH₄ is
14 methanotrophy, and the fact that subsurface waters were depleted of CH₄ suggests that CH₄ consumption
15 is higher than production, or that no production occurs in subsurface waters. Interestingly, although CH₄
16 microbial oxidation occurs throughout the water column and is recognized as an important process that
17 reduces CH₄ emissions (Reeburgh et al., 2007; Rehder et al., 1999), there have been few investigations
18 on microbial communities mediating aerobic CH₄ oxidation. There does exist a few measurements of
19 aerobic CH₄ oxidation in marine environments, and measurements taken from open systems under
20 oligotrophic regimes (Tilbrook and Karl, 1994, Holmes et al., 2000) which report lower levels of
21 oxidation than in the oxic/anoxic interface (Sansone and Martens, 1978 Reeburgh et al., 1991).

22 **4.3. CH₄ and N₂O emission in the southern Ocean**

1 Highly dynamic gas exchanges were registered in the KPR, with source and sink scenarios for N₂O and
2 only a source scenario for CH₄. Since the mean wind speed did not exceed 14 m s⁻¹, LM86 and W92
3 parameterizations represent the more conservative overestimation estimates of gas exchange in the area
4 (Frost and Upstill-Goddard, 2003). The gas inventories in the ML reflect the effect of gas transport
5 mainly via turbulent mixing and advection, which can be accelerated by the action of wind but also by
6 the microbial activity in surface waters. The ML depth did not correlate to wind speed (rs: 0.31, p< 0.05)
7 and this aids to estimate the gases content in the ML and whether it is a result of in situ production or
8 consumption. CH₄ fluxes were higher at stations located at the PF and A3, where phytoplanktonic
9 blooms were observed (see Table 2), but the tendency was the reverse for N₂O, with an influx into the
10 aforementioned stations. CH₄ emission rates during this study were higher than previously measured
11 (Table 2), with a range of 0.1 to 3.0 μmol m⁻² d⁻¹ for the Pacific Ocean (Bates et al., 1996; Holmes et
12 al., 2000; Sansone et al., 2001) and 0.5 to 9.7 μmol m⁻² d⁻¹ for the Atlantic Ocean (Oudot et al.,
13 2002; Forster et al., 2009). In the South Pacific ocean (10°-64°S, 140°E), crossing the PF, Yoshida et
14 al. (2011) reported CH₄ fluxes ranging from 2.4 to 4.9 μmol m⁻² d⁻¹.
15 In the case of N₂O, the estimates in this study were in the expected range for the oligotrophic open ocean
16 (Nevison et al., 1995). N₂O undersaturation and the concomitant influx were estimated, although this
17 situation has not yet been well described for the Southern Ocean. N₂O sinks can occasionally be
18 observed (Butler et al., 1989; Law and Ling, 2001) which can be explained by probable N₂O
19 assimilation by N-fixing microorganisms. This process may be responsible for the estimated N₂O influx.

20

21 **5. Implications**

22 The dynamics of both gases differ substantially both spatially and vertically (surface to 500 m depth),
23 indicating that different mechanisms are being activated to produce an active gas during recycling. Our

1 findings also show that in areas of active fertilization and biogenic particle accumulation, CH₄
2 accumulates while N₂O becomes depleted. This study suggests that the Antarctic Polar Zone plays a
3 significant role in surface CH₄ production and subsequent air-sea gas exchange. These results did not
4 agree with some previous studies of artificial fertilization experiments in the Southern Ocean, although
5 only a few studies of this nature exist. This indicates that the turnover and evolution of microbial
6 communities in mesoscale structures are fundamental for the development of substrates and conditions
7 for CH₄ regeneration. Surface N₂O does not spatially respond to natural iron fertilization, at least in
8 terms of N₂O production via nitrification or that N₂O consumption does not occur any rapider than the
9 N₂O production process. However in subsurface water N₂O accumulation seems to take place via
10 nitrification.

11

12 **Acknowledgements:** We would like to thank the captain and crew of the R/V Marion Dufresne. We
13 recognized the support of both project leaders (Stephane Blain and Bernard Queguiner). This work was
14 supported by the French Research program of INSU-CNRS LEFE-CYBER (Les enveloppes fluides et
15 l'environnement –Cycles biogéochimiques, environnement et ressources), the French ANR (Agence
16 Nationale de la Recherche, SIMI-6 program, ANR-10-BLAN-0614), the French CNES (Centre National
17 d'Etudes Spatiales) and the French Polar Institute IPEV (Institut Polaire Paul-Emile Victor). We are
18 also grateful to Louise Oriol and Stephane Blain for nutrient data and Marine Lasbleiz for the HPLC
19 analysis of chlorophyll measurements. The altimeter and colour/temperature products for the Kerguelen
20 area were produced by Ssalto/Duacs and CLS with support from Cnes. We also recognize all our
21 colleagues that contributed to KEOPS 2. CF and LF were supported by the Proyecto Ecos-Conicyt
22 C09B02 and the International Associated Laboratory MORFUN. CF received partial support from

1 Fondap N°15110027. LF founded the analysis of samples obtained in the KEOPS 2 cruise with
2 FONDECYT N° 1120719. This is a contribution by 15110009 (FONDAP-CONICYT).

3
4 **References**

- 5 Alldredge, A. L. and Y.Cohen. Can microscale chemical patches persist in the sea? Microelectrode study
6 of marine snow, fecal pellets, *Science*, 235, 689–691, doi:10.1126/science.235.4789.689, 1987.
- 7 Arrieta, J.M., Weinbauer, M.G., Lute, C. and Hernd, G.J. Response of bacterioplankton to iron
8 fertilization in the Southern Ocean, *Limnology and Oceanography*, 49(3), 799-808, 2004.
- 9 Bates T.B., Kelly, K.C., Johnson, J.E. and Gammon, R.H. A re-evaluation of the open ocean source of
10 methane to the atmosphere, *Journal of Geophysical Research*, 101 (D3), 6953–6961, 1996.
- 11 Berman-Frank, I., Quigg, A., Finkel Z. V., Irwin A.J., Haramaty, L. Nitrogen-fixation strategies and Fe
12 requirements in cyanobacteria, *Limnology and Oceanography*, 52(5), 2260–2269, 2007.
- 13 Blain, S., Quéguiner, B., Armand, L., Belviso, S., Bombled, B., Bopp, L., Bowie, A., Brunet, C.,
14 Brussaard, K., Carlotti, F., Christaki, U., Corbière, A., Durand, I., Ebersbach, F., Fuda, J.L., Garcia,
15 N., Gerringa, L.J.A., Griffiths, F.B., Guigue, C., Guillerm, C., Jacquet, S., Jeandel, C., Laan, P.,
16 Lefe`vre, D., Lomonaco, C., Malits, A., Mosseri, J., Obernosterer, I., Park, Y.H., Picheral, M.,
17 Pondaven, P., Remenyi, T., Sandroni, V., Sarthou, G., Savoye, N., Scouarnec, L., Souhault, M.,
18 Thuillers, D., Timmermans, K.R., Trull, T., Uitz, J., Van-Beek, P., Veldhuis, M.J.W., Vincent, D.,
19 Viollier, E., Vong, L and Wagener, T. Effect of natural iron fertilization on carbon sequestration in
20 the Southern Ocean, *Nature*, 446 (7139), 1070–1075, 2007.
- 21 Blain, S., Sarthou, G. and Laan, P. Distribution of dissolved iron during the natural iron fertilization
22 experiment KEOPS (Kerguelen Plateau, Southern Ocean), *Deep-Sea Research II*, doi:10.1016/
23 j.dsr2.2007.12.028, 2008.
- 24 Blain, S., Capparos, J., Guéneuguès, A., Obernosterer, I. and Oriol, L. Distributions and stoichiometry of
25 dissolved nitrogen and phosphorus in the iron fertilized region near Kerguelen (Southern Ocean).
26 *Biogeosciences*, 12, 623-635, 2015. doi:10.5194/bg-11-5931-2014
- 27 Blais, M., Tremblay J.-É., Jungblut, A. D., Gagnon, J., Martin, J., Thaler, M. and Lovejoy, C. Nitrogen
28 fixation and identification of potential diazotrophs in the Canadian Arctic. *Global Biogeochemical*
29 *Cycles*, 26, GB3022, doi:10.1029/2011GB004096, 2012
- 30 Butler, J. H., Elkins, J.W., Thompson, T. M and Egan. K.B. Tropospheric and Dissolved N₂O of the
31 West Pacific and East Indian Oceans During the El Niño Southern Oscillation Event of 1987,
32 *Journal of Geophysical Research*, 94, 14865-14877, 1989.
- 33 Cavagna, A.J., Lefèvre, D., Dehairs, F., Elskens, M., Fripiat, F., Closset, I., Lasbleiz, M., Florez-
34 Leiva, L., Cardinal, D., Leblanc, K., Fernandez, C., Oriol, L., Blain, S. and Quéguiner, B.

- 1 Biological productivity regime and associated N cycling in the vicinity of Kerguelen Island area,
2 Southern Ocean . *Biogeosciences Discuss.*, 11, 18073-18104, 2014.
- 3 Chen. L., Zhang, J., Zhan, L., Li, Y., Sun, H. Differences in nitrous oxide distribution patterns between
4 the Bering Sea basin and Indian Sector of the Southern Ocean. *Acta Oceanologica* 33, 9-19, DOI:
5 10.1007/s13131-014-0484-8, 2014.
- 6 Chever, F., Sarthou, G., Bucciarelli, E., Blain, S. and Bowie, A.R.. An iron budget during the natural
7 iron fertilisation experiment KEOPS (Kerguelen Islands, Southern Ocean). *Biogeosciences*, 7: 455-
8 468, 2010.
- 9 Christaki, U., Lefèvre, D, Georges, C., Colombet, J., Catala, P., Courties, C., Sime-Ngando, T.,
10 Blain, S. and Obernosterer, I. Microbial food web dynamics during spring phytoplankton blooms in
11 the naturally iron-fertilized Kerguelen area (Southern Ocean). *Biogeosciences Discuss*, 11, 6985–
12 7028, doi:10.5194/bgd-11-6985-2014, 2014.
- 13 Cicerone, R.J. and Oremland, R.S. Biogeochemical aspects of atmospheric methane, *Global*
14 *Biogeochemical Cycles*, 2, 299–327, 1988.
- 15 Codispoti, L.A and Christensen, J.P. Nitrification, denitrification and nitrous oxide cycling in the eastern
16 Tropical South Pacific Ocean, *Marine Chemistry*, 16, 277-300, 1985.
- 17 Codispoti, L. A., Brandes, J. A. Christensen, J. P. Devol, A.H. Naqvi, S.W.A., Paerl, H. and Yoshinari,
18 T. The oceanic fixed nitrogen and nitrous oxide budgets: Moving targets as we enter the
19 anthropocene?, *Scientia Marina*, 65, 85-105, 2001.
- 20 Damm, E., Helmke, E., Thoms, S., Schauer, U., Nöthing, E., Bakker, K., Kiene, R.P. Methane
21 production in aerobic oligotrophic surface water in the central Arctic ocean, *Biogeosciences*, 7,
22 1099-1108, 2010.
- 23 Dehairs, F, Fripiat, F., Cavagna A.-J. Trull, T. W. Fernandez, C., Davies, D. Roukaerts A.,
24 Fonseca Batista, D. Planchon, F. and Elskens M. Nitrogen cycling in the Southern Ocean
25 Kerguelen Plateau area: evidence for significant surface nitrification from nitrate isotopic
26 compositions. *Biogeosciences Discussion*, 11, 13905-13955, 2014
- 27 Díez, B., Bergman, B., Pedrós-Alió, C., Antó, M. and Snoeijs P. High cyanobacterial *nifH* gene diversity
28 in Arctic seawater and sea ice brine. *Environmental Microbiology Reports* 4, 360–366,
29 doi:10.1111/j.1758-2229.2012.00343.x, 2012.
- 30 d'Ovidio, F., Della Penna, A., Trull, T.W., Nencioli, F., Pujol I., Rio, M. H., Park Y.-H. , Cotté C.,
31 Zhou, M. and Blain S. The biogeochemical structuring role of horizontal stirring: Lagrangian
32 perspectives on iron delivery downstream of the Kerguelen plateau. *Biogeosciences*
33 *Discuss.*, 12, 779-814, 2015.
- 34 Emery, W.J and Thomson, R.E. *Data analysis methods in physical oceanography*, Pergamon Press, 634
35 pp, 1997.

- 1 Farias, L., Fernández, C., Faúndez, J., Cornejo, M. and Alcaman, M.E. Chemolithoautotrophic
2 production mediating the cycling of the greenhouses gases N₂O and CH₄ in an upwelling
3 ecosystem, *Biogeosciences*, 6, 3053-3069, 2009.
- 4 Farias, L., Faundez, J., Fernadez, C., Cornejo, M., Sanhueza, S and Carrasco, C. Biological N₂O fixation
5 in the eastern South Pacific ocean, *PLoS One* 8, e63956, doi:10.1371 /journal.pone0063956, 2013.
- 6 Florez-Leiva, L., Damm, E. and Farías, L. Methane production induced by methylsulfide in surface
7 water of an upwelling ecosystem, *Progress in Oceanography*, doi.org/10.1016/ j.pocean.
8 2013.03.005, 2013.
- 9 Fourquez, M., Obernosterer, I., Davies, D.M., Trull, T.W and Blain, S. Microbial iron uptake in the
10 naturally fertilized waters in the vicinity of Kerguelen Islands: phytoplankton-bacteria interactions.
11 *Biogeosciences Discuss.*, 11, 15053-15086, 2014.
- 12 Frost, T., and Upstill-Goddard, R.C. Meteorological controls of gas exchange at a small English lake,
13 *Limnology and Oceanography*, 47(4), 2002, 1165–1174, 2002.
- 14 Forster, G., Upstill-Goddard, R.C., Gist, N., Robinson, C., Uher, G., Woodward, E.M. Nitrous oxide and
15 methane in the Atlantic Ocean between 50°N and 52°S: Latitudinal distribution and sea--air flux,
16 *Deep-Sea Research II* 56, 964-976, 2009.
- 17 Fuhrman, J.A. and Capone, D.G. Possible biogeochemical consequences of ocean fertilization,
18 *Limnology and Oceanography*, 36, 1951-1959, 1991.
- 19 Grasshoff, J. Methods of seawater analysis. In: Grasshoff K, Ehrhardt M, Kremling K (eds.). *Methods of*
20 *seawater analysis* Verlag chimie Germany, 1983.
- 21 Gonzalez, M.L., Molina, V., Florez-Leiva, L. Cavagna, A.J., Dehairs, F., Farias, L. and Fernandez, C.
22 Nitrogen fixation in the southern ocean: A case of study of the Fe-fertilized Kerguelen region
23 (KEOPS II cruise). *Biogeosciences Discuss.*, 11, 17151-17185, 2014
- 24 Hanson, R.S. and Hanson, T.E. Methanotrophic bacteria, *Microbiology and Molecular Biology Reviews*,
25 60(2), 439-471, 1996.
- 26 Heeschen, U. K., Keir, R. S., Rehder, G., Klatt, O and Suess, E. Methane dynamics in the Weddel Sea
27 determined via stable isotope ratios and CFC - 11, *Global Biogeochemical. Cycles*, 18, GB2012,
28 doi:10.1029/2003GB002151, 2004,
- 29 Holmes, R.H., Aminot, A., Kérouel, R., Hooker, B.A., Peterson, J. A simple and precise method for
30 measuring ammonium in marine and freshwater ecosystems. *Canadian Fisheries and Aquatic*
31 *Sciences*, 56,1801-1808, 1999.
- 32 Holmes, M.E., Sansone, F.J., Rust, T.M. and Popp, B.N. Methane production, consumption, and air-sea
33 exchange in the open ocean: An evaluation based on carbon isotopic ratios, *Global Biogeochemical*
34 *Cycles*, 14, 1 – 10, 2000.

- 1 IPCC, 2013: Climate Change 2013: The Physical Science Basis. Contribution of Working Group I to the
2 Fifth Assessment Report of the Intergovernmental Panel on Climate Change Stocker, T.F., D. Qin,
3 G.-K. Plattner, M. Tignor, S.K. Allen, J. Boschung, A. Nauels, Y. Xia, V. Bex and P.M. Midgley
4 (eds.). Cambridge University Press, Cambridge, United Kingdom and New York, NY, USA, 1535
5 pp.
- 6 Jain, A. K., Briegleb, B.P., Minschwaner, K. and Wuebbles D. J. Radiative forcing and global
7 warming potentials of greenhouse gases, *Journal Geophysical Research*, 105, 20,773–20,790.,
8 2000.
- 9 Jin, X. and Gruber, N. Offsetting the radiative benefit of ocean iron fertilization by enhancing N₂O
10 emissions. *Journal Geophysical Research*, 30,, 2249, doi:10.1029/2003GL018458, 2003.
- 11 Jouandet, M-P., Jackson, G. A., Carlotti, F., Picheral, M.,Stemmann, L. and Blain, S. Rapid formation of
12 large aggregates during the spring bloom of Kerguelen Island: observations and model comparisons
13 *Biogeosciences Discussion.*, 11, 4949–4993, doi:10.5194/bgd-11-4949-2014, 2014.
- 14 Karl, D.M., Tilbrook, B.D. Production and transport of methane in oceanic particulate matter, *Nature*,
15 368, 732–734, 1994.
- 16 Karl, D., Beversdorf, L., Björkman, K.M., Church, M.J., Martinez, A., DeLong, E.F. Aerobic production
17 of methane in the sea, *Nature Geoscience*, 1, 473-478, 2008.
- 18 Kiene, R.P. Linn, L.J. J. Gonzalez,J. M.A. Moran, M.A Bruton, J.A. Dimethylsulfoniopropionate and
19 methanethiol are important precursors of methionine and protein-sulfur in marine bacterioplankton.
20 *Applied and Environmental Microbiology*, 65 (10), 4549–4558, 1999.
- 21 Kirchman, D.I, Hoffman, K.A. Weaver, R. and Hutchins, D.A. Regulation of growth and energetics of a
22 marine bacterium by nitrogen source and iron availability, *Marine Ecology Progress Series*, 250,
23 291-296, 2003.
- 24 Lamontagne, R., Swinnerton, J. W., Linnenbom, V.J. and Smith, W. D. Methane concentrations in
25 various marine environments. *Journal of Geophysical Research*, 78, 5317-5324, 1973.
- 26 Laurenceau, E.C., Trull, T. W., Davies, D. M., Bray, S. G., Doran, J., Planchon F., Carlotti, F.,
27 Jouandet, M.-P., Cavagna, A.-J. , Waite, A. M. and Blain S. The relative importance of
28 phytoplankton aggregates and zooplankton fecal pellets to carbon export: insights from free-drifting
29 sediment trap deployments in naturally iron-fertilised waters near the Kerguelen plateau.
30 *Biogeosciences Discussion*, 11, 13623-13673, 2014.
- 31 Law, C. and Ling, R. Nitrous oxide flux and response to increased iron availability in the Antarctic
32 Circumpolar Current, *Deep Sea Research Part II: Topical Studies in Oceanography*, 48, 2509-2527,
33 2001.
- 34 Lasbleiz, M., Leblanc, K., Blain, S., Ras, J., Cornet-Barthaux, V., Nunige, S.H. and Quéguiner, B.,
35 2014a. Pigments, elemental composition (C, N, P, Si) and stoichiometry of particulate matter, in the

- 1 naturally iron fertilized region of Kerguelen in the Southern Ocean. *Biogeosciences*, 11: 5931–
2 5995, doi:10.5194/bg-11- 5931-2014, 2014
- 3 Liss P.S, Merlivat L. Air-sea gas exchange rates: Introduction and synthesis. In: Buat-Menard P. (ed.),
4 The Role of Air-Sea Exchange in Geochemical Cycling. D. Reidel, Dordrecht, pp. 113-127, 1986.
- 5 Nevison, C., Weiss, R. and Erickson III, D.J. Global oceanic emissions of nitrous oxide, *Journal of*
6 *Geophysical Research*, 100, 15809-15820,1995.
- 7 Nevison, C., Butler, J.H. and Elkins, J.W. Global distribution of N₂O and the DN₂O-AOU yield in the
8 subsurface ocean, *Global Biogeochemical Cycles*, 7 (4), 1119, doi:10.1029/2003GB002068, 2003.
- 9 Mills, M.M., Ridame, C., Davey, M., La Roche, J and Geider, R. Iron and phosphorus co-limit nitrogen
10 fixation in the eastern tropical North Atlantic, *Nature.*, 429, 292–294, 2004.
- 11 Mongin, M., Molina, E. and Trull, T. Seasonality and scale of the Kerguelen plateau phytoplankton
12 bloom: A remote sensing and modeling analysis of the influence of natural iron fertilization in the
13 Southern Ocean, *Deep Sea Research Part II: Topical Studies in Oceanography*, 55(5-7), 880-892,
14 2008.
- 15 Moore, C.M , Mills, M.M., Achterberg, E.P., Geider., R J. LaRoche, J., Lucas, MI., McDonagh, E.L.,
16 Pan, X., Poulton, A.J., Rijkenberg, M J. A., Suggett, D.J., Ussher, S. J. and Woodward, E.M.S.
17 Large-scale distribution of Atlantic nitrogen fixation controlled by iron availability, *Nature*
18 *Geoscience*, 2, 867–871, 2009.
- 19 Morel, F.M.M. and Price, N.M. The biogeochemical cycles of trace metals in the Oceans, *Science*, 300,
20 944, DOI: 10.1126/science.1083545, 2003a.
- 21 Morel, F. M. M., Milligan, A.J. and Saito M.A. Marine Bioinorganic Chemistry: The Role of Trace of
22 Metals in the Oceanic Cycles of Major Nutrients in *Treatise on Geochemistry*, Vol. 6, edited by
23 KK. Turekian, H.D. Holland, Elsevier Science Ltd, Cambridge, UK, p. 113-143, 2003b
- 24 Oudot, C., Jean-Baptiste, P., E. Fourreb, E. Mormichea, C. Guevela, M., Ternonc, J.-F , Le Corred, P.
25 Transatlantic equatorial distribution of nitrous oxide and methane, *Deep-Sea Research I*, 49,1175–
26 1193, 2002.
- 27 Oschlies, A., W. Koeve W., Rickels W., and Rehdanz, K. Side effects and accounting aspects of
28 hypothetical large-scale Southern Ocean iron fertilization, *Biogeosciences* 7, 4017–4035, 2010.
- 29 Park, Y-H and Vivier, F. Circulation and hydrography over the Kerguelen Plateau. *Marine ecosystems*
30 *and fisheries*, 5, 43-55, 2012.
- 31 Park, Y.-H., Durand, I., Kestenare, E., Rougier, G., Zhou, M., d’Ovidio, F., Cotté, C. and Lee, J.-H.
32 Polar Front around the Kerguelen Islands: An up-to-date determination and associated circulation
33 of surface/subsurface waters. *Journal Geophysical Research- Oceans*, 119:
34 doi:10.1002/2014JC010061, 2014.

- 1 Qu  rou  , F., Sarthou, G., Chever, F., van der Merwe, P., Lannuzel, D., Townsend, A., Bucciarelli, E,
2 Planquette, H., Cheize, M., Blain, d'Ovidio, F. and A. Bowie, A. A new study of natural Fe
3 fertilization processes in the 2 vicinity of the Kerguelen Islands (KEOPS 2 experiment), KEOPS 2
4 Biogeoscience discussion 12, 231-279, 2015.
- 5 Rees, A.P., Owens, N.J.P and Upstill-Goddard, R.C. Nitrous oxide in the Bellingshausen Sea and Drake
6 Passage, *Journal of Geophysical Research*, 102, 3383– 3391, 1999.
- 7 Reeburgh, W.S, Ward, B.B, Whalen, S.C., Sandbeck, K.A., Kilpatrick, L.J and Kerkhof, K. Black Sea
8 methane geochemistry, *Deep-Sea Research II* (38) S1189–S1210, 1991.
- 9 Reeburgh, W.S. Oceanic methane biogeochemistry. *Chemical Reviews* 107, 486–513, 2007.
- 10 Rehder, G., Keir, R.S., Suess, E., Rhein, M. Methane in the northern Atlantic controlled by microbial
11 oxidation and atmospheric history, *Geophysical Research Letters* 26, 587–590, 1999.
- 12 Rhee, T. S., Kettle, A. J and Andreae, M. O. Methane and nitrous oxide emissions from the ocean: A
13 reassessment using basin-wide observations in the Atlantic, *Journal of Geophysical Research*,
14 114,D12304, doi:10.1029/2008JD011662, 2009.
- 15 Sanial, V., van Beek, P., Lansard, B., Souhaut, M., Kestenare, E., and d'Ovidio, F.: Radium isotopes to
16 track sediments-derived inputs of the Kerguelen Plateau, *Biogeosciences*, *Biogeosciences*
17 *Discuss*, 11, 14023-14061, 2014
- 18 Sansone F.J. and Martens, C.S. Methane oxidation in Cape Lookout Bight, North Carolina, *Limnology*
19 *and Oceanography*, 23, 349–355, 1978.
- 20 Sansone, F.J., Popp, B.N., Gasc, A. Graham, W. Rust, T.M. Highly elevated methane in the eastern
21 tropical North Pacific and associated isotopically enriched fluxes to the atmosphere, *Geophysical*
22 *Research Letters*, 28 4567–4570, 2001.
- 23 Sarmiento, J.L. and Gruber, N. *Ocean Biogeochemical Dynamics*. Princeton University Press, 2006.
- 24 Scranton, M.I and Brewer, P. Occurrence of methane in the near-surface waters of the western
25 subtropical North Atlantic, *Deep-Sea Research*, 24, 127-138, 1977.
- 26 Sim  , R., Archer, S.D., Pedr  -Ali  , C., Gilpin, L., Stelfox-Widdicombe, C.E. Coupled dynamics of
27 dimethyl- sulfoniopropionate and dimethylsulfide cycling and the microbial food web in surface
28 waters of the North Atlantic, *Limnology and Oceanography*, 47, 53–61, 2002.
- 29 Sun, J., Steindler, L. J. Thrash, C. , Halsey, K.H., Smith, D.P. Amy E. Carter, A.E. , Zachary C.
30 Landry, Stephen J. Giovannoni. One Carbon Metabolism in SAR11 Pelagic Marine Bacteria. *PloS*
31 *one* DOI: 10.1371/journal.pone.0023973, 2011.
- 32 Tilbrook, E.D and Karl, D.M. Dissolved methane distributions, sources, and sinks in the western
33 Bransfield Strait, Antarctica, *Journal of Geophysical Research*, 99, 16383–16393, 1994.

- 1 Tréguer P, Le Corre P Manuel d'analyse des sels nutritifs dans l'eau de mer Utilisation de
2 l'AutoAnalyztr 2 Technicon, 2nd edn. 'Univ Bretagne occidentale, Brest, 1975.
- 3 Turner, S.M., Harvey, M. J., Law, C. S., Nightingale, P.D and Liss P.S. Iron-induced changes in oceanic
4 sulfur biogeochemistry, *Geophysical Research Letter*, 31, L14307, doi:10.1029/2004GL020296,
5 2004.
- 6 van der Merwe, P., Bowie, A.R., Quéroué, F., Armand, L., Blain, S., Chever, F., Davies, D., Dehairs, F.,
7 Planchon, F., Sarthou, G. et al., 2014. Sourcing the iron in the naturally-fertilised bloom around the
8 Kerguelen Plateau: particulate trace metal dynamics. *Biogeosciences Discussion*, 11: 13389–13432,
9 doi:10.5194/bgd-11-13389, 2014.
- 10 Vila-Costa, M., Simó, R., Harada, H., Gasol, J.M., Slezak D. and Kiene, R.P. Dimethylsulfoniopropionate
11 uptake by marine phytoplankton, *Science*, 314, 652, 2006.
- 12 Vissher, P.T. ,Kiene, R.P., Taylor B.F. Demethylation and cleavage of demethylsulfoniopropionate in
13 marine intertidal sediments, *FEMS Microbiology Ecology*, 14 179–190, 1994.
- 14 Walter, S., Peeken, I., Lochte, K and Bange, H.W. Nitrous oxide measurements during EIFEX, the
15 European Iron Fertilisation Experiment in the subpolar South Atlantic Ocean, *Geophysical
16 Research Letter*, 32, L23613,doi: 10.1029/2005GL024619, 2005.
- 17 Wingenter, O.W., Haase, K.B., Strutton, P., Friedrich, G., Meinardi, S., Blake, D.R and Rowland, F. S.
18 Changing concentrations of CO, CH₄, C₅H₈, CH₃Bt, CH₃I and dimethyl sulfide during the Southern
19 Ocean Iron Enrichment Experiments, *Proceedings of the National Academy of Sciences* 101, 8537–
20 8541, 2004.
- 21 Wanninkhof, R. Relationship between wind speed and gas exchange over the ocean, *Journal
22 Geophysical Research*, 97, 7373-7382, 1992.
- 23 Weisenburg, D.A and Guinasso, N.L. Equilibrium solubilities of methane, carbon monoxide and
24 hydrogen in water and seawater, *Journal of Chemical Engineering Data*, 24, 354-360, 1979.
- 25 Weiss, R.F. and Prince, B. A. Nitrous oxide solubility in water and seawater, *Marine Chemistry* 8, 347-
26 359, 1980.
- 27 Weller D.I., Law, C.S., A. Marriner, A., Nodder S.D., Chang, F.H., Stephens, J.A., Wilhelm S.W.,
28 Boyd P.W., Sutton P.J.H. Temporal variation of dissolved methane in a subtropical mesoscale
29 eddy during a phytoplankton bloom in the southwest Pacific Ocean, *Progress in Oceanography*,
30 116, 193–206, 2013.
- 31 Wolfe, R.S. Microbial formation of methane, *Advance Microbial Physiology*, 6, 107–146, 1971.
- 32 Wuebbles, D.J and Hayhoe, K. Atmospheric methane and global change, *Earth-Science Reviews*, 57,
33 177–210, 2002.

1 Yoch, D. Dimethylsulfoniopropionate: Its Sources, Role in the Marine Food Web, and Biological
 2 Degradation to Dimethylsulfide Applied Environmental Microbiology 2002; 68(12), 5804–5815,
 3 2002. doi: 10.1128/AEM.68.12.5804-5815, 2002.

4 Yoshida, O., Inoue, H. Y., Watanabe, S, Suzuki, K. and Noriki, S. Dissolved methane distribution in
 5 the South Pacific and the Southern Ocean in austral summer J. Geophysical Research 116, C07008,
 6 2011, doi:10.1029/2009JC006089, 2011.

7 Zhou, M., Zhu, Y., d'Ovidio, F., Park, Y.-H., Durand, I., Kestenare, E., Sanial, V., Van-Beek, P.,
 8 Queguiner, B., Carlotti, F., and Blain, S.: Surface currents and upwelling in Kerguelen Plateau
 9 regions, Biogeosciences Discussion, 11, 6845–6876, 2014.

10

11

12 **Figure caption**

13

14 Figure 1. Map showing the location of biogeochemical stations sampled during the KEOPS 2 cruise.
 15 Bathymetric topography is shown in the main oceanographic region. The orange line delimits the
 16 position of the polar front. The transects are indicated.

17

18 Figure 2. Left column: a) Temperature ($T^{\circ}\text{C}$), c) Salinity and e) T-S diagram for E-W transect. Station
 19 located close to the PF (purple) is shown, showing enhanced water mass mixing. Arrows indicate
 20 position of PF crossing this transect. Right column: b) Temperature ($T^{\circ}\text{C}$), d) Salinity and f) T-S
 21 diagram for the TEW .

22

23 Figure 3. Vertical cross section of a) nitrate ($\mu\text{mol L}^{-1}$); b) phosphate ($\mu\text{mol L}^{-1}$); c) chlorophyll-a (μg
 24 L^{-1}); d) dissolved oxygen ($\mu\text{mol L}^{-1}$), e) nitrous oxide (nmol L^{-1}) and f) methane (nmol L^{-1}) for zonal
 25 transect between $69\text{-}75^{\circ}\text{E}$. Arrows indicate position of PF crossing this transect

26

27 Figure 4. Vertical cross section of a) nitrate ($\mu\text{mol L}^{-1}$); b) phosphate ($\mu\text{mol L}^{-1}$); c) chlorophyll-a (μg
 28 L^{-1}); d) dissolved oxygen ($\mu\text{mol L}^{-1}$), e) nitrous oxide (nmol L^{-1}); f) methane (nmol L^{-1}) for the
 29 meridional transect between $45^{\circ}\text{-}51^{\circ}\text{S}$.

30

31 Figure 5. PCA analysis with environmental data including dissolved iron obtained in the zonal transect
 32 (TEW). PCA comprises a) data from the surface to the base of the ML and b) environmental data from
 33 the surface to 500 m depth. Stations along with the eigenvectors are included.

34

35 Figure 6. Vertical distribution of biogeochemical variables from selected stations. Different
 36 biogeochemical regimes are defined as HNLC area (St. R), northern and southern area of Polar front (St.
 37 TNS-1 and A3-2) and close to the Polar front (Sts. TEW-3 and TEW-7).

38

39

Table 1. General oceanographic features of the sampled stations during the KEOPS 2 cruise

Biogeochemical Provinces	Stations	Latitude	Longitude	Date	Bottom Depth	MLD	Temperature	Salinity	Oxygen
		°S	°E	mm-dd-yy	(m)	(m)	(°C)		($\mu\text{mol L}^{-1}$)
	OISO-6	-44.59	52.06	10-15-11	3260	110	3.68 (3.66-3.68)	33.80 (33.80-33.81)	317.4 (314-318)
	OISO-7	-47.4	58.00	10-16-11	4300	127	4.75 (4.73-4.76)	33.79 (33.8-33.81)	308.4 (305-309)
N-S transect									
	A3-1	-50.38	72.05	10-19-11	535	181	1.68 (1.68-1.73)	33.89 (33.85-33.91)	325.9 (321-327)
	A3-2	-50.38	72.05	10-16-11	527	165	2.16 (2.10-2.18)	33.91 (33.911-33.913)	333.2 (329-335)
	TNS10	-50.12	72.07	10-21-11	565	163	1.67 (1.59-1.68)	33.90 (33.80-33.93)	325.9 (314-327)
Eddy	TNS-9	-49.47	72.12	10-21-11	615	137	1.75(1.66-1.89)	33.91(33.80-33.84)	321.1 (265-331)
Eddy	TNS-8	-49.27	72.14	10-21-11	1030	139	2.11 (2.06-2.12)	33.869 (33.86-33.87)	329.4 (324-328)
	TNS-7	-49.08	72.17	10-22-11	1890	62	2.10 (1.95-2.16)	33.86 (33.86-33.87)	327.7 (327-331)
	TNS-6	-48.48	71.18	10-22-11	1885	67	2.32 (2.23-2.42)	33.846 (33.84-33.85)	327.6 (315-316)
	TNS-5	-48.28	72.12	10-22-11	2060	114	2.22 (2.09-2.26)	33.85 (33.85-33.86)	326.7(323-328)
	TNS-3	-47.05	71.55	10-23-11	540	111	2.17 (2.06-2.26)	33.89(33.88-33.89)	307.6(304-310)
	TNS-2	-47.19	71.42	10-23-11	520	65	3.60 (3.38-3.67)	33.69 (33.68-33.69)	318.6 (317-319)
	TNS-1	-46.49	71.30	10-23-11	2280	45	4.02(3.96 -4.13)	33.71(33.71-33.72)	316.1 (315-318)
HNLC	R-2	-50.21	66.43	10-23-11	2300	111	2.11 (2.06-2.14)	33.78 (33.77-33.78)	326.7 (326-327)
E-W transect									
(Shelf)	TEW-1	-49.08	69.50	10-31-11	86	16	3.27 (3.17-3.36)	33.61(33.61-33.62)	344.16 (340-345)
(Shelf)	TEW-2	-48.53	70.39	10-31-11	84	40	2.55 (2.49-2.68)	33.75 (33.75-33.76)	332.0 (327-337)
(Shelf)	TEW-3	48.47	71.01	10-31-11	565	62	2.17 (2.12-2.31)	33.86 (33.86-33.87)	329.69 (328-331)
	TEW-4	-48.37	71.28	11-01-11	1585	95	2.54 (2.41-2.60)	33.85 (33.85-33.86)	334.60 (331-337)
	TEW-5	48.28	72.47	11-01-11	2275	60	2.51 (2.39-2.60)	33.84 (33.84-33.85)	331.42 (327-336)
(NPF)	TEW-7	-48.27	73.59	11-02-11	2510	17	4.02 (3.91-4.10)	33.78 (33.784-33.79)	315.95 (346-349)
	TEW-8	-48.28	75.19	11-02-11	2786	22	4.15 (4.08-4.18)	33.76 (33.76-33.77)	338.75(347-350)
Time Series Stations									
	E-1	-48.27	72.11	10-28-11	2056	84	2.48 (2.36-2.54)	33.85(33.84-33.85)	331.54(328-333)
	E-2	-48.31	72.04	11-01-11	2003	42	2.42 (2.28-2.56)	33.85 (33.85-33.86)	331.68 (329-333)
	E-3	-48.48	71.58	11-03-11	1915	41	2.74 (2.60-2.81)	33.84 (33.84-33.85)	332.08 (331-332)
	E-4W	48.45	71.25	11-11-11	1384	67	2.36 (2.07-2.51)	33.90 (33.90-33.91)	329.95 (326-332)
	E-4E	48.42	72.33	11-12-11	2210	77	3.15 (2.78-3.19)	33.84 (33.83-33.85)	329.89 (326-331)
	E-5	48.24	71.50	11-18-11	1920	36	2.53 (2.50-2.62)	33.85 (33.85-33.85)	326.97(330-333)

Table 2. Inventories of gases and nutrients estimated in the mixed layer (ML) and the entire water column, along with GHG concentrations, wind velocities and concomitant estimated gas exchange across the air-sea interface

Station	Inventory in the ML					Inventory in the Water Column				GHGs		Wind m s ⁻¹	Flux LM86		Flux W92	
	*Chl- <i>a</i> mg m ⁻²	CH ₄ mmol m ⁻²	N ₂ O mmol m ⁻²	NO ₃ ⁻ mol m ⁻²	PO ₄ ³⁻ mol m ⁻²	N ₂ O mmol m ⁻²	CH ₄ mmol m ⁻²	NO ₃ ⁻ mol m ⁻²	PO ₄ ³⁻ mol m ⁻²	N ₂ O nM	CH ₄ nM		N ₂ O μmol m ⁻² d ⁻¹	CH ₄ μmol m ⁻² d ⁻¹	N ₂ O μmol m ⁻² d ⁻¹	CH ₄ μmol m ⁻² d ⁻¹
N-S Transect																
A3-1	12.60	3.00	2.43	5.41	0.293	5.72	4.12	7.342	0.940	13.73	6.56	6.58	-1.54	18.75	-2.96	35.93
A3-2	35.48	3.31	1.81	4.38	0.300	5.273	3.31	15.04	1.024	11.64	8.,37	11.39	-10.5	14.24	-22.9	29.70
TNS10	14.09	1.39	2.56	4.79	0.319	9.29	2.17	16.03	1.077	15.49	7.79	12.66	3.57	14.90	6.56	27.48
TNS-9	35.58	1.33	2.23	3.91	0.254	7.51	1.87	12.53	0.864	15.89	14.54	14.38	5.08	38.10	9.36	70.26
TNS-8	23.23	0.68	2.16	3.98	0.260	9.27	1.58	15.75	1.038	15.46	5.65	11.89	4.29	7.80	7.92	14.38
TNS-7	25.45	0.25	1.02	1.69	0.111	9.99	1.80	15.74	1.072	16.92	4.01	11.89	8.65	2.03	15.55	3.66
TNS-6	16.33	0.57	0.92	1.83	0.123	8.65	2.54	15.93	1.070	13.81	8.74	11.89	-0.78	17.59	-1.20	31.64
TNS-5	17.19	0.74	1.68	3.07	0.212	9.27	2.46	15.39	1.070	14.67	6.41	11.40	1.81	9.91	3.26	17.82
TNS-3	17.28	0.88	1.75	3.06	0.214	7.75	3.14	12.46	0.875	11.05	7.23	11.40	4.13	9.93	6.85	16.44
TNS-2	11.25	0.26	0.91	1.73	0.123	8.27	1.57	15.08	1.046	13.92	4.38	9.73	1.48	3.03	2.45	5.00
TNS-1	11.21	0.39	0.63	1.07	0.076	8.89	3.16	14.17	0.976	13.95	8.48	9.73	2.26	14.40	3.74	23.84
R-2	14.89	0.64	1.63	2.79	0.197	2.83	1.06	4.900	0.347	14.83	6.29	6.86	0.89	4.09	1.34	6.15
W-E Transect																
TEW-1	9.78	0.19	0.26	3.40	0.412	1.18	1.30	1.560	0.111	15.29	9.50	4.60	0.87	3.15	1.69	6.15
TEW-2	9.87	0.43	0.62	0.84	1.073	1.12	1.74	1.873	0.133	15.03	9.88	4.60	0.54	3.24	1.06	6.33
TEW-3	8.77	0.73	0.91	0.51	1.566	7.41	2.40	14.97	1.072	15.56	14.09	4.60	0.67	5.25	1.32	10.24
E--2	15.33	0.52	0.20	0.82	1.167	9.78	2.80	15.24	1.051	14.95	11.42	6.92	1.34	11.67	2.01	17.57
TEW-4	35.53	0.40	1.63	0.30	2.468	10.3	1.81	15.74	1.106	16.62	3.50	6.92	3.76	0.21	5.67	0.32
TEW-5	23.11	0.38	0.99	0.52	1.619	10.21	2.61	15.62	1.099	16.31	6.35	6.92	3.28	4.34	4.94	6.54
TEW-7	75.45	0.19	0.23	2.39	0.353	9.26	7.44	15.23	1.087	12.90	10.87	8.04	-0.96	15.42	-1.52	23.78
TEW-8	59.52	0.10	0.37	1.52	0.472	10.05	1.59	15.27	1.058	15.77	4.95	8.04	5.25	3.52	8.10	5.42

*Inventories estimated from the photic zone

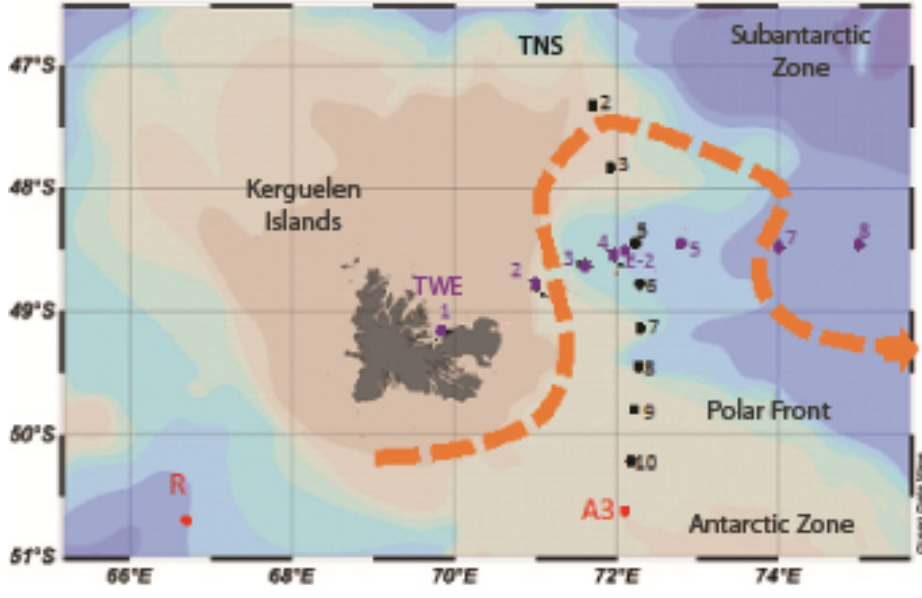


Figure 1

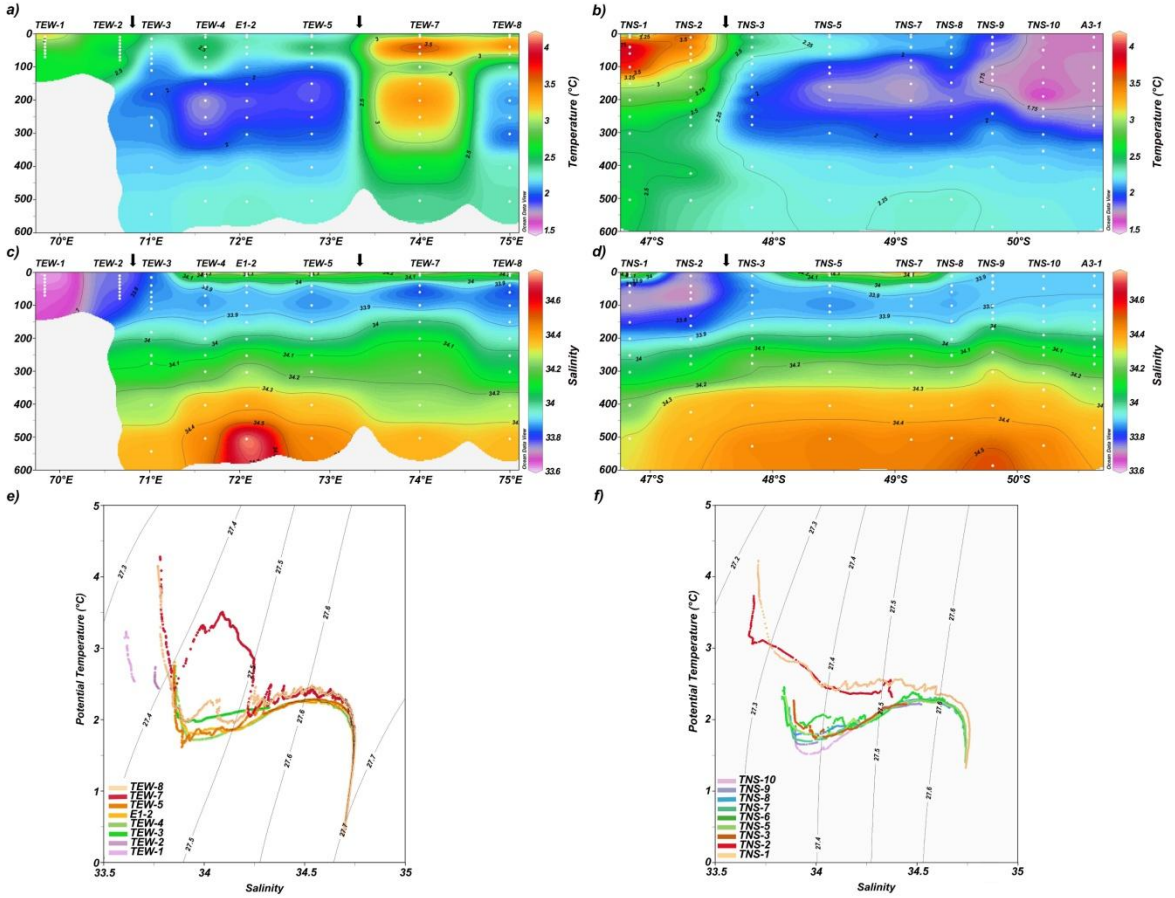


Figure 2

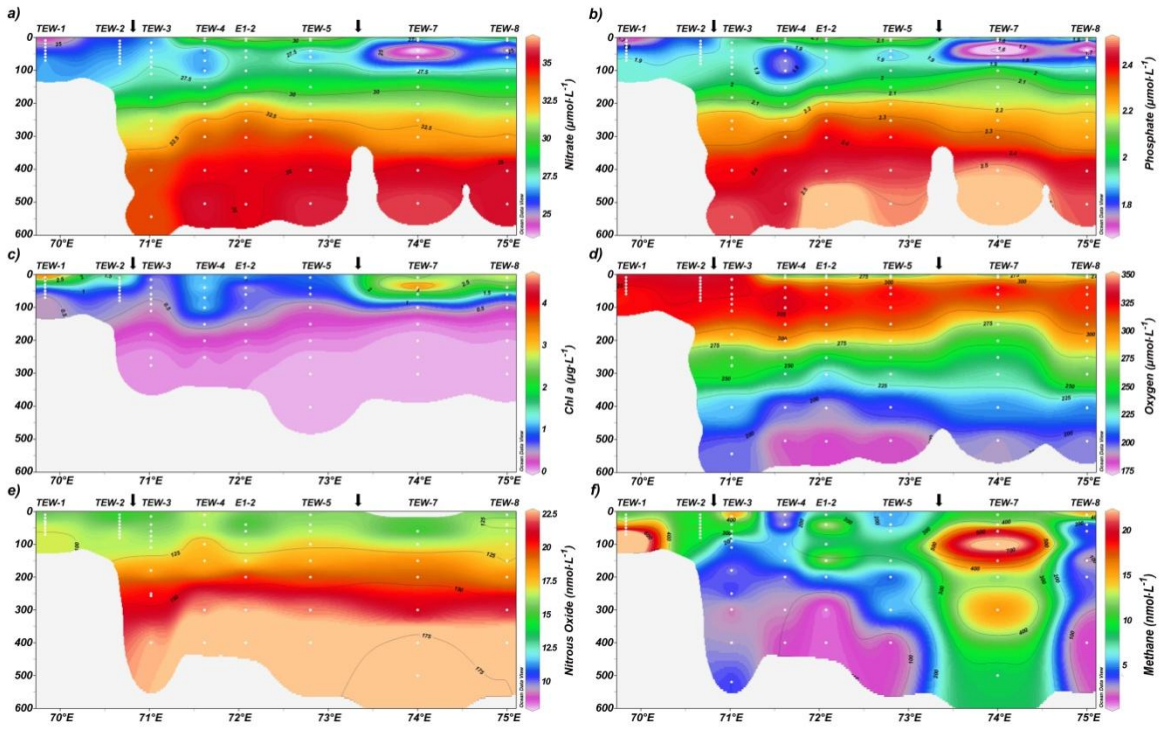


Figure 3

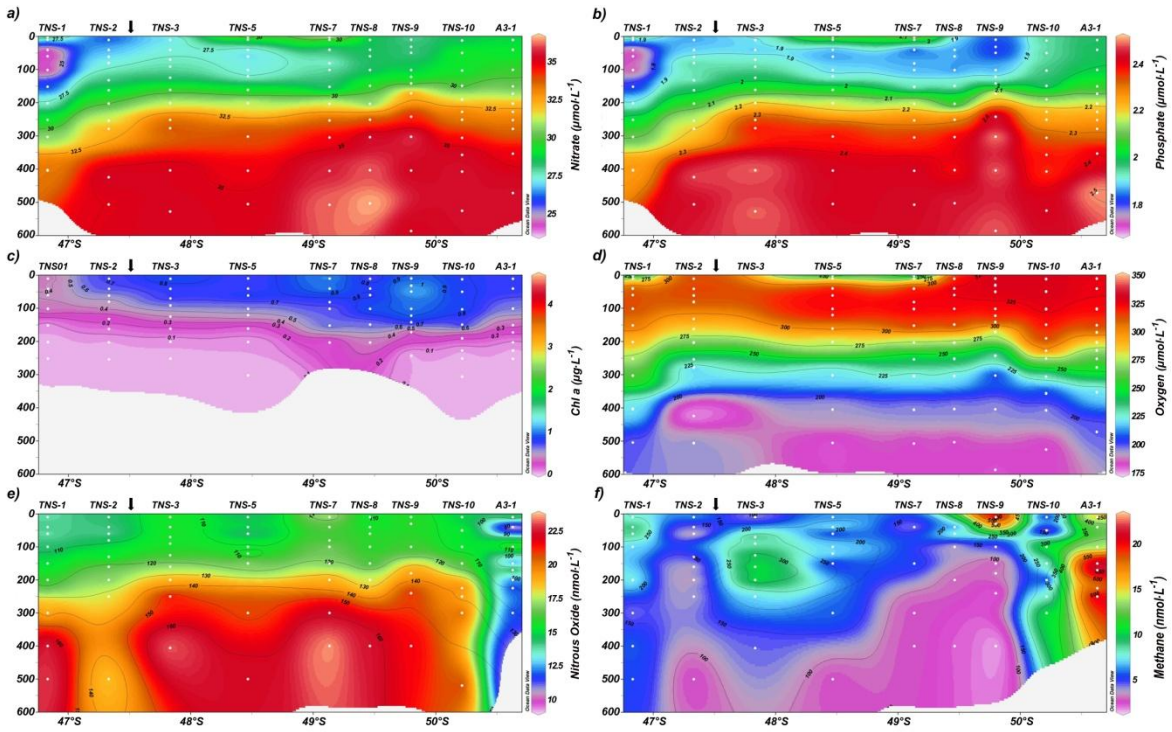


Figure 4

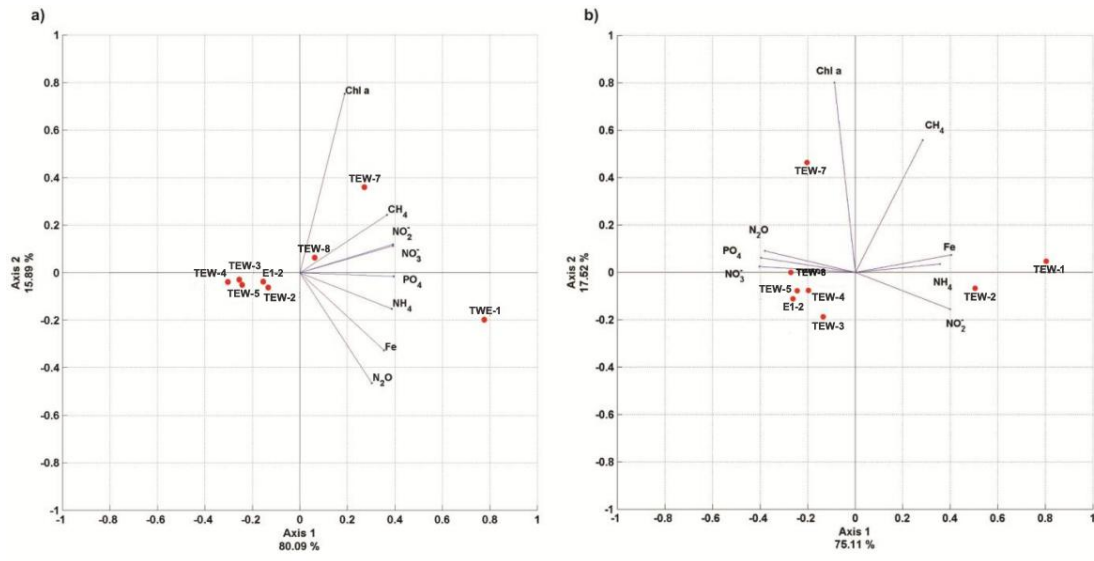


Figure 5

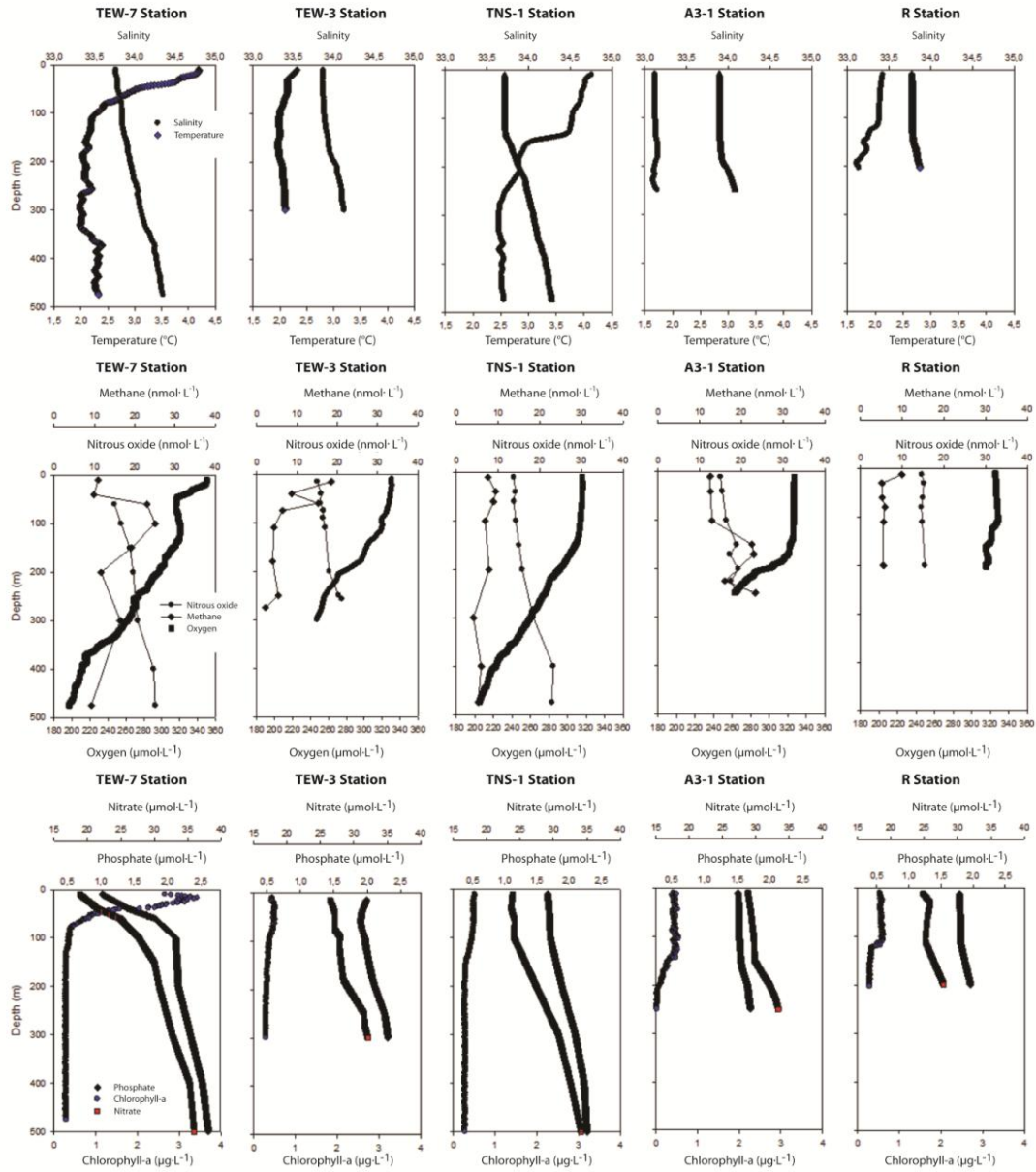


Figure 6

